TITLE:

Purified Zymogens Reveal Mechanisms of Snake Venom Metalloproteinase Auto-Activation

AUTHORS:

Sophie Hall[1], Iara Aimê Cardoso[1], Mark C. Wilkinson[2], Maria Molina Carretero[3], Srikanth Lingappa[1], Bronwyn Rand[1], Dakang Shen[1], Johara Boldrini-França[1], Richard Stenner[1], Stefanie K. Menzies[2,4], Georgia Balchin[1], Konrad Kamil Hus[1,5], Renaud Vincentelli[6], Andrew Mumford[3], Alastair W. Poole[7], Nicholas R. Casewell[2], Imre Berger[1,8]*, Christiane Schaffitzel[1]*

AFFILIATIONS:

[1] School of Biochemistry, University of Bristol, University Walk, Bristol BS8 1TD, UK

[2] Centre for Snakebite Research and Interventions, Liverpool School of Tropical Medicine, Liverpool L3 5QA, UK

[3] School of Cellular and Molecular Medicine, University of Bristol, 1 Tankard's Close, Bristol BS8 1TD, UK

[4] Lancaster University, Bailrigg, Lancaster, United Kingdom

[5] Department of Biotechnology and Bioinformatics, Faculty of Chemistry, Rzeszow University of Technology, Powstancow Warszawy 6, 35-959 Rzeszow, Poland

[6] Architecture et Fonction des Macromolécules Biologiques (AFMB), UMR 7257 CNRS-Aix-Marseille Université, 13288 Marseille, France

[7] Bristol Medical School, University of Bristol, University Walk, Bristol BS8 1TD, UK

[8] Max Planck Bristol Centre for Minimal Biology, School of Chemistry, University of Bristol, Cantock's Close, Bristol BS8 1TS, UK

For Correspondence:

Christiane Schaffitzel, email: christiane.berger-schaffitzel@bristol.ac.uk

Imre Berger, email: imre.berger@bristol.ac.uk

ABSTRACT

Snake venoms contain diverse mixtures of toxins that evolved to incapacitate prey, but in humans they cause extensive pathology following snakebite envenomation. In viper venom, some of the most potent toxins are the haemorrhagic and coagulopathic snake venom metalloproteinases (SVMPs). Because venoms contain a SVMP cocktail, and due to their cytotoxicity, SVMP characterizations have been hampered by the lack of purified enzymes. By incorporating their prodomain, which blocks the active SVMP site, we overcame their cytotoxicity and enabled recombinant production of zymogens from all three structurally variable SVMP classes (PI, PII and PIII) using our baculovirus/insect cell expression system. Zymogens were auto-activated by incubation with Zn^{2+} ions, resulting in prodomain cleavage, PII disintegrin cleavage and PIII prodomain proteolysis. Auto-activated SVMPs were characterized using protein substrate degradation, platelet aggregation and blood coagulation assays, benchmarked to native venom-purified SVMP. Our recombinant zymogen production protocol is generically applicable for the expression of SVMPs, unlocking biomedical use in haematology, and discovery of novel snakebite therapeutics.

INTRODUCTION

Snake venom is a complex cocktail of more than 100 proteins and peptides belonging to various toxin families (*1*). Although the number and abundance of isoforms within these families vary extensively across different venomous snakes, the snake venom metalloproteinases (SVMP) are a pathologically important toxin family present in almost all snake venoms. SVMPs play a significant role in the physiological effects resulting from both local and systemic envenoming, such as haemorrhage, coagulopathy and tissue necrosis (*2*). In many medically important viperid snake genera such as *Echis* (saw-scaled vipers), SVMP toxins are the most abundant toxin constituents, on average accounting for 33% of all toxins, though this can be as high as 72% in *Echis ocellatus* (*3-5*) (Fig. 1a).

SVMPs are complex, structurally variable, cysteine-rich, Zn^{2+}-dependent metalloproteinases that can be classified into three sub-classes based on domain architecture: PI (comprising metalloproteinase domain only), PII (metalloproteinase and disintegrin domains) and PIII (metalloproteinase, disintegrin-like and cysteine-rich domains) (Fig. 1b); representatives of all three sub-classes are present in different viper venoms (*6*) (*7*).

SVMPs are particularly toxic proteins with a wide range of substrates. They are known to degrade the basement membrane and extracellular matrix proteins, as well as several blood clotting factors, most notably fibrinogen, through their metalloproteinase domain (*8, 9*). Extracellular matrix breakdown and loss in blood capillary wall integrity results in vascular leakage, resulting in both local and systemic haemorrhage (*10*) and in the spread of other venom toxins (*11*). In PII SVMPs, the disintegrin domain contains a charged, integrin-binding motif, most commonly an arginine-glycine-aspartate (RGD) motif, which binds, among others, the fibrinogen receptor integrin $\alpha_{IIb}\beta_3$ (*12*), causing inhibition of platelet aggregation.

Because viper SVMPs often target components of the coagulation cascade with unique specificity and/or lack of reliance on typically essential co-factors, these enzymes are highly valuable for investigating and monitoring the treatment of pathologies related to haemostasis (e.g. factor deficiencies, bleeding disorders) (*13*). In the clinic, the SVMPs RVV-X and Ecarin are both used as standards for coagulation tests (*14*). In addition, SVMP-derived disintegrins have been repurposed for use as, or inspiration for the design of, anti-platelet therapies to treat atherothrombosis in the form of unstable angina and myocardial infarction (*1*). Thus, a single snake venom toxin family has yielded several translationally valuable tools for diagnosis and treatment of human disease. However, further exploitation of SVMPs is hampered by the considerable challenge in purifying individual SVMP proteins from venom, and the lack of robust, scalable, recombinant toxin production protocols, representing a bottleneck.

52 Currently, SVMPs are typically purified from venom by size exclusion chromatography (SEC),
53 followed by ion exchange chromatography of the peaks containing SVMPs. Further
54 separation can be achieved by hydrophobic interaction chromatography or reversed-phase
55 high performance liquid chromatography (RP-HPLC) (*15, 16*). However, complete separation
56 of endogenous functionally active SVMPs is difficult to achieve, because: (i) many venoms
57 contain multiple related SVMP isoforms that share similar physicochemical properties, (ii) the
58 resulting yields of each particular SVMP isoform can be very low, and (iii) the use of some
59 desirable separation approaches (e.g. RP-HPLC) can result in SVMP denaturation.
60 Importantly, this procedure is impeded by the limited access to sufficient amounts of
61 extracted snake venom.

62 Recombinant expression of SVMPs could resolve the bottleneck, but is severely hampered
63 by their cytotoxicity, domain complexity and high number of cysteine residues that
64 complicate protein folding - for example, the PIII SVMPs contain between 20 and 40
65 cysteines forming disulfides (*17*). Currently, protocols are available for the production of only
66 a select few specific SVMPs (including albocollagenase, bothropasin and Ecarin) (*18-20*).
67 However, these suffer from limitations such as low yield and inactive proteins. Zymogen
68 production of SVMPs has been described before, but it remains generally elusive how the
69 zymogen is processed into the mature, active SVMP. Current protocols describe incubation
70 of the zymogen for >7 days (*20*), incubation with other active proteinase toxins (*21*), or the
71 insertion of a TEV protease cleavage site into the SVMP amino acid sequence (*22*).

72 Here, we establish a novel and generic protocol to access functional PI, PII and PIII SVMPs
73 in the quality and quantity required for characterizations and show that all three classes of
74 SVMPs can auto-activate in the presence of zinc ions, resulting in distinct outcomes.

75 We used our MultiBac baculovirus/insect cell expression system (*23*) for recombinant SVMP
76 zymogen production. The MultiBac system is well-established for secretion of proteins,
77 including the C-terminal heavy chain domain of the highly toxic protein, clostridial botulinum
78 neurotoxin (*24*). We postulate that this system is highly suitable for SVMP production
79 because (i) folding of the multi-domain SVMP zymogen will be supported by eukaryotic,
80 endogenous chaperones present in insect cells and (ii) secreted SVMPs will undergo cellular
81 protein quality control in the endoplasmic reticulum (ER) and Golgi apparatus for correct
82 disulfide bond formation and glycosylation before secretion, ensuring that the toxins
83 produced are correctly folded, soluble and authentically modified. We show that zymogen
84 expression overcomes SVMP cytotoxicity, and we demonstrate successful production of PI
85 and PII SVMPs from *Echis ocellatus* and a PIII SVMP from *Echis carinatus sochureki*
86 (Fig. 1b,c). We establish auto-activation of the SVMP zymogens and concomitant cleavage
87 of the prodomain (all classes), C-terminal tags (PI, PII) and the disintegrin domain (PII). The

88 PIII prodomain is completely degraded by the activated SVMP. We further analyse the
89 cytotoxicity and haemotoxicity of the auto-activated SVMPs *in vitro* using established casein
90 (*25*), fibrinogen (*25*), fluorogenic peptide (*26*) and insulin degradation (*15*) assays. For the PI
91 SVMP, we show that the substrate specificity of recombinant SVMP is identical to that of the
92 corresponding toxin purified from venom, compellingly validating the utility of our strategy.

93 Our generic SVMP production protocol thus paves the way to systematically characterize
94 SVMPs and unlock biomedical applications, in haematology, thrombosis and inflammation
95 research and as targets for the discovery of novel snakebite therapeutics.

96 **RESULTS**

97 **Recombinant SVMP zymogen expression overcomes their cytotoxicity.**

98 For our expression trials, we chose PI, PII and PIII SVMPs which, according to
99 transcriptomics (*27*), are highly expressed in the venom gland of medically important saw-
100 scaled vipers. We generated baculovirus/insect cell expression constructs for Q2UXQ3 (PI),
101 A0A3G1E3U2 (PII) and E9JG34 (PIII) (Fig. 1c), each encoding a signal sequence for
102 secretion, the toxin of interest and C-terminal tandem octa-histidine- and Avi-tags, codon
103 optimized for both *Spodoptera frugiperda* and *Trichoplusia Ni* as expression hosts (Fig. S1).
104 Initially, recombinant production of mature SVMPs, without the N-terminally fused prodomain,
105 was attempted (Fig. S2a). Protein expression yields, however, were extremely low, primarily
106 due to SVMP cytotoxicity causing pervasive cell death immediately upon baculoviral
107 infection due to initial trace amounts of SVMP. Subsequent expression strategies to produce
108 SVMPs were aimed at inactivating the metalloproteinase by adding an inhibitor, native
109 propeptides or SVMP active site mutants (Supplementary text). Marimastat, a broad-
110 spectrum metalloproteinase inhibitor (*28*) could not prevent cell death induced by PIII SVMP
111 expression. On the contrary, the cell viability in the presence of 3 μM and 6 μM Marimastat
112 was even further decreased (Fig. S2b). Similarly, active site mutants in the PIII SVMP still
113 showed significant toxicity, markedly reducing yellow fluorescent protein (YFP) levels, which
114 serve as a proxy for heterologous protein production, as well as cell viability (Fig. S2c).

115 In the snake venom gland, SVMPs are produced with an N-terminally fused prodomain that
116 is removed through cleavage during post-translational processing of the protein (Fig. 2a).
117 The prodomain comprises a small, highly conserved propeptide sequence (usually
118 PKMCGVT) - this propeptide acts as a cysteine switch to maintain enzyme latency (*29*).
119 AlphaFold 3 (*30*) predicts that the prodomain adopts a β-barrel structure and folds around
120 the metalloproteinase (MP) domain, slotting the propeptide into the active site of the MP
121 domain, where the propeptide cysteine co-ordinates the active site Zn^{2+} ion, along with the
122 three active site histidines (Fig. 2a). This renders the MP inactive as the Zn^{2+} ion cannot be
123 accessed by substrates in the active site.

124 Inspired by this, we designed propeptide-SVMP fusion proteins with three propeptide
125 repeats to the N-terminus of the SVMP followed by a TEV protease cleavage site. We
126 hypothesized that this would increase the avidity of the propeptide to the MP active site and
127 efficiently inactivate the enzyme. While cell viability and YFP fluorescence levels for PI and
128 PIII slightly increased (Fig. S2d), compared to expression of the mature SVMP (Fig. S2a),
129 YFP expression was still significantly lower as compared to a positive control which
130 expressed an unrelated, non-toxic protein. Western blot analysis confirmed soluble

131 expression of PI and PIII SVMPs (Fig. S2d), but protein yields in the media remained too low
132 to progress to purification.

133 Therefore, we produced complete SVMP zymogens, where the native signal sequence and
134 the entire prodomain including propeptide is expressed N-terminally to the MP domain (Fig.
135 2, Fig. S1), adopting a compact structure as predicted by AlphaFold 3 (*30*) (Fig. S3). Cells
136 expressing PI, PII and PIII SVMPs as zymogens showed clearly improved cell viability,
137 remaining above 60% on day 4 of expression (Fig. 2b). PIII SVMP zymogen was harvested
138 on day 4 to avoid additional cell death and lysis. In contrast, the cells expressing PI and PII
139 SVMPs remained ~75% viable on day 5 of expression when the SVMPs were harvested.
140 Notably, the zymogen-expressing cells had considerably higher YFP readings as compared
141 to the cells previously expressing mature PI and PIII SVMPs, and no loss of YFP
142 fluorescence over time was observed (Fig. 2c). Western blot analysis using an anti-His-tag
143 antibody confirmed the presence of PI, PII and PIII zymogens in cell extract and lysate; and
144 zymogen protein was also detected in the concentrated media fraction, indicating successful
145 secretion (Fig. 2d). We conclude that SVMPs require the full-length N-terminal prodomain to
146 ensure enzyme latency is maintained, and to allow for significant amounts of protein to be
147 produced and secreted when recombinantly expressed using a baculovirus/insect cell
148 system.

149 **SVMP zymogens can be produced in milligram amounts.**

150 Following secretion of the SVMP zymogens into the media, a three-step purification was
151 performed (Fig. S1). Firstly, cells were pelleted by centrifugation, and the media containing
152 secreted proteins were passed through a HiTrap IMAC column for metal affinity purification
153 to enrich the secreted SVMPs from the comparatively large culture media volume. SVMPs
154 were eluted using imidazole. Fractions containing SVMP zymogen were dialyzed and further
155 purified by anion exchange chromatography (IEX), followed by size exclusion
156 chromatography (SEC). SVMP zymogens generally eluted in one prominent peak in SEC
157 (Fig. 3).

158 Notably, dialysis following IMAC affinity purification of PI SVMP resulted in self-cleavage of
159 the zymogen as evidenced by a downward shift of the PI protein band in the SDS-PAGE gel
160 from 55 kDa to 45 kDa before and after dialysis, respectively (Fig. S4a). Western Blot
161 analysis indicated a loss of the His-tag after dialysis (Fig. S4b). The protein was confirmed to
162 be PI SVMP by mass spectrometry (Fig. S4c,d). The observed auto-activation of PI SVMP is
163 likely due to residual metal ions in the insect cell media and buffers, trace metal ions
164 leaching off the resin during IMAC purification, and/or a change in pH from the cell culture
165 medium at pH 6 to the purification buffer at pH 8, which is the pH recommended for binding
166 to the IMAC column - the lower pH of the medium being similar to that of the venom gland

167 (pH 5.4), which helps maintain enzyme latency (*31*). The PI SVMP zymogen without the C-
168 terminus (including the Avi-tag and His-tag), eluted from the SEC column in one peak at
169 14.8 ml, corresponding to a calculated molecular weight (MW) of ~50 kDa which agrees with
170 the predicted MW for the monomeric zymogen (Fig. 3a). The yield of purified PI SVMP
171 zymogen was 0.63 mg from a 1 L Hi5 insect cell culture.

172 Following observation of the loss of the SVMP PI C-terminus during purification, a new
173 protein construct was designed with the Avi- and His-tags fused C-terminally to the observed
174 proteolytic degradation site as suggested by MW loss seen by SDS-PAGE and based on
175 AlphaFold 3 models (*30*), giving rise to a shorter construct named PIΔC. In fact, this new C-
176 terminus of the MP domain aligns with that of fully characterized PI SVMPs found in venom
177 (*32-34*). During PIΔC IMAC affinity purification, the zymogen (predicted MW: 45.4 kDa)
178 underwent partial activation, resulting in cleavage between the MP (theoretical MW: 26.2
179 kDa) and prodomain (theoretical MW: 19.3 kDa) (Fig. S5a). Subsequent IEX allowed for the
180 isolation of a small amount of PIΔC MP domain alone, however the bulk of the PIΔC MP
181 remained bound to the prodomain, forming a stable complex despite cleavage. The PIΔC
182 MP domain alone eluted from the SEC column at a MW of ~29 kDa, corresponding to the
183 MW expected for the monomeric MP domain (Fig. S6a). The PIΔC metalloproteinase in
184 complex with the prodomain eluted from the SEC column in a different peak corresponding
185 to a MW of ~48 kDa, confirming that the cleaved prodomain and MP domain form a stable
186 assembly with a 1:1 stoichiometry (Fig. S6b). The yield of PIΔC was 0.44 mg for the MP
187 domain and 3.25 mg for the MP with non-covalently bound prodomain from a 1 L Hi5 insect
188 cell culture.

189 The PII SVMP zymogen was purified as intact zymogen and did not undergo any (self-)
190 cleavage throughout purification (Fig. 3b). In SEC, a small amount of protein eluted in the
191 void volume, likely due to the very high concentration of PII zymogen when loaded onto the
192 column, possibly causing some aggregation. The majority of PII SVMP zymogen eluted with
193 a small peak corresponding to ~198 kDa (p2) and a large, sharp peak corresponding to ~84
194 kDa (p3). SDS-PAGE analysis with non-reducing loading dye suggests that peak p2
195 corresponds to a PII zymogen dimer (Fig. S7a,b). Peak p3 corresponds to the monomeric
196 PII SVMP zymogen, which has a predicted MW of 56 kDa, in agreement with its elution
197 volume in SEC. The yield of PII SVMP zymogen was 8.3 mg (peak 3) from a 1 L Hi5 insect
198 cell culture.

199 The PIII SVMP zymogen underwent partial activation during the purification process, similar
200 to that of PIΔC SVMP. This was observed following elution from the IMAC column (Fig. S5b)
201 and resulted in the presence of three bands in SDS-PAGE (Fig. 3c), corresponding to the
202 PIII zymogen (predicted MW 70.2 kDa), mature PIII SVMP (MP domain, disintegrin-like

203 domain and cysteine-rich domain) with a predicted MW of 50.6 kDa, and the prodomain with
204 a MW of 19.6 kDa. Interestingly, despite the processing of some PIII molecules, the protein
205 still eluted in one peak from the SEC, at a MW of ~108 kDa based on the elution volume.
206 This indicates that the prodomain again remains associated with the mature SVMP following
207 cleavage, as previously observed for the PIΔC SVMP (Fig. S5a). The yield of the PIII SVMP
208 was 2.2 mg from a 1 L Hi5 insect cell culture.

209 We observed a difference in the calculated MW based on SEC elution volume (~108 kDa)
210 and the predicted MW (70 kDa) for the PIII SVMP zymogen. Similarly, the PIII zymogen and
211 mature PIII SVMP both run at a higher-than-expected MW on SDS-PAGE (~80 kDa and ~60
212 kDa, respectively). In order to explain this difference in apparent MW of the PIII SVMP, we
213 analysed the proteins for the presence of N-glycans. The NetNGlyc 1.0 server predicts 2
214 glycosylation sites in the mature PIII SVMP (*35*), and we tested all purified SVMP zymogens
215 for glycosylation using Peptide:N-glycosidase F (PNGase F) (Fig. S8). The bands
216 corresponding to PI and PII SVMPs did not change in the presence of PNGase F. However,
217 we observed a downward shift in the MW of the bands corresponding to the PIII zymogen
218 and mature PIII SVMP protein in SDS-PAGE following treatment with PNGase F. De-
219 glycosylation of PIII proteins produced bands at ~77 kDa and ~57 kDa, closer to their
220 predicted MWs (Fig. S8c). We thus confirmed glycosylation of our recombinant PIII SVMP,
221 accounting for the observed higher MW. Due to unavailability of the corresponding native PIII
222 SVMP from *E. carinatus sochureki*, a more detailed comparative analysis of glycosylation
223 and comparison of glycosylation patterns between native and recombinant PIII SVMP is
224 precluded.

225 In conclusion, by using the protocol we have developed, we can produce highly purified
226 recombinant SVMP zymogens, each in mg quantities per liter expression culture.

227 **Co-expression of protein disulfide isomerases does not improve SVMP zymogen**
228 **yields or folding.**

229 Transcriptomic studies have shown that snake venom glands overexpress several
230 chaperones alongside venom toxins, in particular protein disulfide isomerases (PDI), heat
231 shock proteins and calreticulin (*36*). These chaperones are expected to be essential for the
232 correct folding of complex, disulfide-rich toxins. In particular, PDIs assist in the formation,
233 breakage and rearrangement of disulfide bonds, stabilizing the proteins. Successful folding
234 of venom peptides aided by PDI was previously demonstrated for marine cone snails (*37*).
235 Furthermore, overexpression of PDI during recombinant protein expression has been shown
236 to increase overall protein yield (*38*). Therefore, co-expression of SVMPs with PDI could
237 increase SVMP protein yields enabling more protein to be correctly folded and secreted,
238 potentially reducing protein aggregation. To test our hypothesis, we co-expressed the PII and

239 PIII SVMP zymogens with two PDIs: a human PDI (UniProt ID: P07237) and a snake PDI
240 (from *Echis ocellatus*) (*27*), the latter is overexpressed in venom gland tissue (Fig. S9a).
241 Contrary to our expectations, PDI overexpression in insect cells did not noticeably enhance
242 the expression or folding of our SVMP zymogens, and we did not observe increased SVMP
243 yield or activity (Fig. S9 and Supplementary text).

244 **Auto-activation of SVMP zymogens reveals cleavage of the prodomains, the PII**
245 **disintegrin domain and PIII prodomain degradation.**

246 Cleavage of the prodomain in native zymogens is thought to result in the removal of the
247 propeptide from the active site rendering it accessible to substrates, with Zn^{2+} as an
248 essential cofactor. We thus hypothesized that activation of our purified zymogens could be
249 achieved by addition of Zn^{2+} ions. Therefore, we incubated the SVMPs with Zn^{2+} ions at
250 37°C for 18 hours and optimized the Zn^{2+} concentration for activation for each SVMP (Fig.
251 3d-f).

252 The PI SVMP zymogen could be close to completely activated by 750 μM $ZnCl_2$ (Fig. 3d).
253 When analysed by SDS-PAGE, the ~45 kDa band corresponding to the zymogen mostly
254 disappears, and two lower MW bands of ~23 kDa and ~26 kDa appear, corresponding to the
255 prodomain and MP domain, respectively. The two proteins could not be separated under the
256 native conditions of SEC, indicating that the prodomain remains stably bound to the MP
257 domain, despite cleavage (as observed for PIΔC, Fig. S6b). Separation of the MP and
258 prodomain has occurred during SDS-PAGE, however, due to the denaturing and thiol-
259 reducing conditions used. AlphaFold 3 generated models (*30*) (Fig. 2a) suggest the
260 prodomain is located on the opposite side of the MP domain, distal from the active site. Thus,
261 the bound prodomain is not expected to interfere with the ability of the metalloproteinase to
262 bind and cleave substrates, once the propeptide has been detached from the active site. It is
263 interesting to note that the C-terminal part of the PI SVMP zymogen was cleaved during
264 buffer exchange by dialysis while the zymogen was still intact (Fig. S3a) and assumed to be
265 inactive. The observed C-terminal cleavage could be due to a few auto-activated PI SVMPs
266 or due to contaminating proteases from insect cells still present in the affinity purified protein
267 fractions.

268 The truncated PIΔC SVMP construct was almost completely cleaved into mature protein
269 during purification, however this protein was not fully active in our assays. For full activity,
270 the PIΔC SVMP was incubated with 450 μM $ZnCl_2$ leading to significantly higher activity in
271 casein assays (Fig. S6c). Despite complete cleavage of the zymogen, the resulting
272 prodomain and MP domain could not be separated, as was the case for the full-length PI,
273 and, thus, no MP was isolated from this construct either (Fig. S10). Because this PIΔC

274 SVMP corresponds better to the processed, native version of PI SVMP protein, PIΔC was
275 used in all further activity assays and is referred to as PI SVMP from here on.

276 The PII SVMP zymogen was completely activated by 750 μM $ZnCl_2$ (Fig. 3e). Notably, when
277 analysed by SDS-PAGE, a clear separation of prodomain and mature protein was not
278 observed. The band migrating at ~40 kDa corresponds to MP and disintegrin (confirmed by
279 Western blot, Fig. S7c). This band disappears with higher concentrations of Zn^{2+} and/or
280 longer incubation times. The band migrating at ~8 kDa is thought to correspond to the
281 processed disintegrin domain but could not be confirmed by Western blot due to loss of C-
282 terminal tags during activation. After incubation for 1 week, only the 8 kDa and 23 kDa bands
283 remained (Fig. 3e). Based on apparent MW, these bands correspond to the disintegrin and
284 prodomain, respectively. In summary, PII SVMP has undergone further processing to remove
285 the tags and disintegrin from the MP domain, and the MP domain appears to be unstable
286 over time.

287 The PIII SVMP zymogen was completely activated by the addition of 150 μM $ZnCl_2$ (Fig. 3f)
288 as evidenced by the disappearance on SDS-PAGE of the ~77 kDa band corresponding to
289 the zymogen. Instead, the band strengthened at ~60 kDa corresponding to the mature
290 SVMP (MP domain plus disintegrin-like domain and cysteine-rich domain) together with a
291 band at ~25 kDa corresponding to the prodomain. Notably, at higher concentrations of Zn^{2+},
292 the C-terminal tags and the prodomain band are degraded by the PIII SVMP.

293 We conclude that all SVMP zymogens studied can auto-activate by incubation with Zn^{2+},
294 leading to cleavage of the prodomain from the zymogen. In the case of PIΔC and PIII
295 SVMPs the prodomain remains associated with the SVMP at low Zn^{2+} concentrations. After
296 Zn^{2+} activation, the C-terminal tags and the PIII prodomain are degraded by the activated
297 SVMPs, and in the case of PII SVMP, further proteolysis occurs into the constituent parts.

298 **Casein and fibrinogen degradation assays demonstrate SVMP activity.**

299 Degradation of casein is a general protease activity assay that is used in functional assays
300 for all SVMP classes (*25*). SVMP zymogens were supplemented with optimal concentrations
301 of $ZnCl_2$ for SVMP activation (Fig. 3d-f) and incubated with 0.525 μg/μl (~23 μM) casein
302 overnight at 37°C. The degradation of casein was analysed by SDS-PAGE; indicated
303 concentrations relate to input SVMP zymogen concentrations (Fig. 4a-f). The PI SVMP
304 degraded casein (Fig. 4a); activity was observed when adding 73 nM PI and complete
305 degradation of casein occurred at the addition of 1.17 μM PI. The PII SVMP exhibited weak
306 activity against casein (Fig. 4b), which may be due to the self-degradation of the MP domain
307 observed during Zn^{2+} activation (Fig. 3e). Casein degradation was observed when adding
308 1.36 μM PII, as evidenced by the emergence of lower MW bands (Fig. 4b). The PIII SVMP

309 was active against all casein chains (Fig. 4c), with activity seen from concentrations as low
310 as 21 nM PIII, and complete digestion of casein was observed with 343 nM PIII.

311 Next, we performed fibrinogen degradation assays followed by SDS-PAGE analyses (Fig.
312 4d-f). None of our recombinant SVMPs had very strong activity against the γ chain of
313 fibrinogen, as is usually the case with SVMPs (*34*). However, PI, PII and PIII SVMPs
314 degraded Aα and Bβ chains of fibrinogen to different extents.

315 The majority of PI SVMP activity was directed against the Aα chain of fibrinogen (Fig. 4d),
316 with the lowest amount of enzyme tested (73 nM). At higher concentrations of PI (585 nM),
317 activity towards the Bβ chain was also observed. Therefore, PI SVMP can be classified as
318 an alpha/beta fibrinogenase, with a preference for the Aα chain. PII SVMP caused removal
319 of fibrinopeptide B (FpB) from the Bβ chain (Fig. 4e) at a concentration of 134 nM. At higher
320 concentrations (268 nM or more), the Aα chain was also degraded. Thus, PII SVMP is an
321 alpha/beta fibrinogenase with a preference for the Bβ chain. PIII SVMP degraded the Aα
322 chain of fibrinogen at the lowest concentration of PIII tested, 21 nM (Fig. 4f). When
323 supplementing 85 nM PIII or more, the band at 60 kDa corresponding to the Bβ chain
324 disappears as well. Thus, we classify PIII SVMP as an alpha/beta fibrinogenase, with a
325 preference for the Aα chain.

326 To summarize, all recombinant SVMPs (PI, PII, PIII) degraded casein, confirming their
327 activity. They also degraded the alpha and beta chains of fibrinogen in a fibrinogenolytic
328 manner, rather than cleaving fibrinopeptides in a thrombin-like manner.

329 **Auto-activated PIII SVMP shows high substrate affinity and catalytic efficiency.**

330 We next tested if the SVMPs cleave a quenched fluorogenic substrate, ES010 (R & D
331 Systems) which is commonly used to study SVMPs (*39*) and matrix metalloproteinases (*40*)
332 for small molecule therapeutic discovery. PIII SVMP was able to cleave the Gly-Leu bond in
333 ES010 (Fig. 4g). In contrast, SVMPs PI and PII did not effectively cleave this PIII SVMP and
334 MMP-prototypic substrate under the conditions tested (Fig. S11a). For the PIII SVMP, the
335 rate of reaction (monitored by fluorescence increase) was plotted against varying substrate
336 concentrations (ranging from 0 μM to 180 μM), and a Michaelis-Menten curve was
337 calculated (Fig. 4g). The low K_M of 19.6 μM indicates a high binding affinity of the PIII SVMP
338 for the ES010 fluorogenic substrate. The high catalytic efficiency (k_{cat}/K_M) of 3.26 x10^7 $M^{-1}s^{-1}$
339 further suggests that the PIII SVMP is highly effective and specific in processing this
340 substrate. For comparison, a k_{cat}/K_M value of 4,471 $M^{-1}s^{-1}$ was reported for matrix
341 metalloproteinase MMP10 for an ESO10-derived peptide (*41*), and k_{cat}/K_M values of 30,000
342 $M^{-1}s^{-1}$ for a triple-helical peptide for MMP-2 (*42*). Together, these parameters demonstrate

343 that the recombinant PIII SVMP exhibits both strong substrate affinity and high catalytic
344 efficiency towards this prototypical PIII SVMP substrate.

345 **Native and recombinant PI SVMP exhibit the same substrate specificity in insulin B**
346 **degradation assays.**

347 Next, we assayed the activity of SVMPs PI, PII and PIII against insulin B, a test substrate
348 used previously in SVMP characterization (*15*). Degradation of insulin B at multiple sites was
349 visualized by RP-HPLC. PI and PIII showed distinct insulin B degradation patterns indicating
350 different sequence specificities and cleavage sites while the PII SVMP did not degrade
351 insulin B (Fig. S11b). PIII SVMP cleaves insulin B into 6 products (Fig. 4h). PI SVMP cleaves
352 insulin B into 5 products (Fig. 4i). While we could not purify the native PII and PIII SVMPs
353 from *Echis* venom for comparative purposes, the native PI SVMP can be readily purified
354 from *Echis ocellatus* venom (*43*). Therefore, we could compare insulin B cleavage by our
355 recombinant PI SVMP with insulin B cleavage by the native source-purified PI enzyme.
356 Identical degradation products of insulin B were observed (Fig. 4i). Thus, our recombinant PI
357 SVMP is active and has the same substrate specificity as the native enzyme from venom,
358 underscoring that our recombinant expression strategy leads to native-like SVMPs,
359 compellingly validating our approach.

360 **PII zymogen and activated PII SVMP inhibit platelet aggregation.**

361 Some haemorrhagic SVMPs can disrupt cell adhesion and prevent haemostasis by
362 interfering with platelet aggregation (*44*). SVMPs with either a disintegrin (PII), or disintegrin-
363 like domain (PIII) can inhibit platelet aggregation through a motif found in these domains.
364 Most commonly, this corresponds to a RGD sequence, which binds integrins. Binding of
365 disintegrin to integrin $\alpha_{IIb}\beta_3$ can be measured through inhibition of 2-MeS-ADP-induced
366 platelet aggregation whereby turbidity is determined by plate aggregometry (Fig. 5a). When
367 tested at a concentration of 500 nM SVMP, platelet aggregation was reduced to 12% and 36%
368 by the activated PII SVMP and the zymogen form, respectively, confirming that the
369 disintegrin is active and capable of inhibiting platelet aggregation. Based on our results, the
370 presence of the prodomain in the zymogen has low inhibitory effect on the RGD-containing
371 disintegrin domain, as anticipated. In comparison, the PI and PIII SVMPs did not inhibit 2-
372 MeS-ADP-induced platelet aggregation (Fig. 5a). The PI SVMP lacks the disintegrin domain
373 and instead of an RGD motif, the PIII SVMP has a divergent 'RSECD' motif in its disintegrin-
374 like domain, which most likely does not interact with integrin $\alpha_{IIb}\beta_3$. We conclude that our
375 recombinant PII SVMP inhibited platelet aggregation, confirming disintegrin activity in the
376 context of both the zymogen and also the activated PII SVMP.

377 **PIII SVMP has no pro-coagulant activity in thrombin clot time assays.**

378 Thrombin clot time assays measure the time required for thrombin to convert fibrinogen to
379 fibrin, leading to clot formation. This assay is used in the clinic to highlight abnormalities in
380 fibrinogen and fibrin clot formation. In our assays, thrombin was replaced with each SVMP to
381 identify the thrombin-like activity of the enzyme. The assay measures turbidity, which is
382 plotted against time. The first and second derivatives are plotted on the same graph, and the
383 maximum rate of change of turbidity (the peak in the 2nd derivative) indicates the time of clot
384 formation. When thrombin is added, fibrin clot formation requires 16.5 seconds (Fig. 5b). As
385 a positive control and example of pro-coagulant SVMPs, thrombin was replaced with native
386 PIII SVMPs purified from *Echis ocellatus* venom. Fibrin clot formation occurs in 28.1 seconds
387 in the presence of the *Echis ocellatus* PIII SVMPs (Fig. 5c), confirming clot formation and
388 pro-coagulation activity. However, when replaced with the recombinant PIII SVMP (from
389 *Echis carinatus sochureki*) no clot formation occurs (Fig. 5d). Similarly, PI and PII SVMPs do
390 not cause blood clotting (Fig. 5e, Fig. S11c). This shows that our recombinantly produced
391 SVMPs have no pro-coagulant activity, which was reported previously for the PI SVMP (*43*)
392 but remained unknown for the PII and PIII SVMPs.

393 **PI and PIII SVMPs are cytotoxic.**

394 HaCaT cells (immortalized human keratinocyte cells), commonly used in dermatological,
395 toxicological and cancer research, were incubated with PI, PII and PIII SVMPs for 24 hours,
396 and cytotoxicity was monitored using the MTT (3-(4,5-dimethylthiazol-2-yl)-2,5-
397 diphenyltetrazolium bromide) assay (*45*). At the tested concentration, PII SVMP showed
398 minimal cytotoxicity (Fig. 5f). In comparison, at 100 µg/mL the PI and PIII SVMPs were
399 clearly cytotoxic, with cell viability decreasing by 40% and 50% after 24 hours, respectively
400 (Fig. 5f). The cytotoxic effect of our PIII SVMP (*Echis carinatus sochureki)* (100 µg/ml) is
401 comparable to that of crude *Echis carinatus* venom on HEK 293T cells, which induces 63%
402 cytotoxicity with 100 µg/ml venom after 3 hours (*46*). Published IC_{50} values for HaCaT cells
403 treated with whole venom for 24 hours fall between 10 and 100 µg/ul (*47*), however it is
404 important to highlight the distinction between the complex cocktail of toxins found in venom
405 and the homogenous, purified SVMP evaluated in this study.

406 **DISCUSSION**

407 The characterization of SVMP toxins, critical for effective bioprospecting and the discovery of
408 snakebite therapeutics, is severely hampered by difficulty in isolating the native proteins from
409 venom. Here, we established a generic protocol for efficient recombinant production of the
410 three structurally diverse classes of SVMPs as zymogens, which overcomes this obstacle.
411 We demonstrate expression of PI, PII and PIII SVMP zymogens from *Echis* species in high
412 quality and quantity using the MultiBac baculovirus/insect cell expression system.

413 In SVMP zymogens, the highly conserved propeptide sequence which blocks the active site
414 of the MP domain, is clamped in place by the N-terminal prodomain. It should be noted that
415 despite expression as a zymogen, residual cytotoxicity was still observed, evident by the
416 decrease in cell viability throughout expression and reduction in the amount of co-expressed
417 YFP fluorescence due to cell lysis (Fig. 2). In agreement with this observation, PI and PIII
418 SVMPs were able to partially activate themselves, resulting in the presence of three
419 characteristic bands in Coomassie-stained SDS-gels – the zymogen, mature SVMP and
420 prodomain. We speculate that this auto-cleavage could be due to the SVMP active site
421 accreting divalent metal ions from the media and buffers used. Additionally, it is likely that the
422 change in pH from 6 (expression) to 8 (purification) allows the activation of SVMPs, as is the
423 case when venom is released from the venom gland (pH 5.4) into the victim (pH 7.4) during
424 envenoming (*31*). A complete control of self-activation of SVMP zymogens would be highly
425 desirable. However, previous studies reported that (i) SVMP zymogens are processed within
426 secretory cells of the venom gland (*48*), and that (ii) mature SVMPs accumulate in secretory
427 vesicles during venom production (*49*). Accordingly, complete prevention of SVMP zymogen
428 auto-processing will be very difficult to achieve because this would require Zn^{2+} ion depletion
429 within the cells which would result in cytotoxicity.

430 Of note, despite the self-cleavage of the PI and PIII zymogens, the majority of the mature
431 SVMP protein remained associated with the prodomain. Interestingly, this did not affect the
432 activity of the SVMPs. According to AlphaFold 3 structure predictions, the prodomain is
433 located on the side of the MP domain, which is opposite to the active site. Upon activation,
434 cleavage of the prodomain releases the propeptide from the active site. This renders the
435 Zn^{2+} ion in the active site free to interact with a substrate. In agreement, we observe that the
436 SVMPs are active even if the prodomain, now no longer covalently linked to the SVMP,
437 remains bound to the MP domain (Fig. 3c, Fig. S5).

438 SVMP zymogens undergo additional post-translational processing: The PI SVMP construct
439 described here was based on transcriptomic data and corresponds to the UniProt sequence
440 ID: Q2UXQ3. During purification, it underwent C-terminal truncation by ~10 kDa, leading to a
441 smaller protein which corresponds closely to previously characterized PI SVMPs (*32-34*).

442 Moreover, we observed a general trend of loss of C-terminal tags during purification,
443 activation and subsequent activity assays for all three SVMP classes.

444 Here, we show that the recombinant PIII SVMP comprises N-linked glycosylation. We would
445 like to point out that when expressed in insect cells, the glycosylation pattern may be
446 different compared to endogenous SVMPs due to differences in the snake and insect
447 glycosylation pathways. The Sf21 and Hi5 cells used in this study typically produce N-
448 glycans that are trimmed to a core 'paucimannose' structure (Man3GlcNAc2), often with an
449 alpha1,6-fucosylation (*50*). While snakes can produce more complex, sialylated N-glycans,
450 glycomic studies of native venoms (e.g. *Bothrops* venoms) have demonstrated that high-
451 mannose and paucimannose structures are also prevalent in native SVMPs (*51*). Therefore,
452 the recombinant glycoforms likely represent a subset of the native glycan heterogeneity and
453 not the full diversity found in snake venom toxins. Moreover, Sf21 and Hi5 cells recognize
454 the same N-glycosylation sequon (Asn-X-Ser/Thr) as reptilian cells, and therefore the site-
455 occupancy remains consistent with the native protein, preserving the overall topography of
456 the toxin.

457 To improve SVMP yields and/or activity, we hypothesized that co-expression of SVMPs with
458 human or snake PDI would aid their proper folding, ensuring the multiple disulfide bonds
459 were correctly formed. Based on transcriptomic data from *Echis* venom gland (*27*), PDIs are
460 highly overexpressed in the snake venom gland. However, PDI over-expression in insect
461 cells did not improve protein yields nor enzyme activity. We speculate that the endogenous
462 insect cell PDIs are sufficient for SVMP folding in our setup. Alternatively, a combination of
463 different chaperones may be required for further boosting SVMP production.

464 SVMP zymogens from all three classes could be auto-activated by the addition of Zn^{2+} ions.
465 While some PI SVMP was processed during purification, any remaining PI zymogen could
466 be cleaved into the mature SVMP and prodomain by incubation with Zn^{2+}. The PII zymogen
467 could be activated by the same means, although there was no clear separation into
468 prodomain and mature protein. Instead, we observed two bands corresponding to the
469 disintegrin and prodomain after prolonged incubation with Zn^{2+} (Fig. 3e). It is unlikely that the
470 observed disappearance of the MP domain is due to misfolding because the PII zymogen is
471 well expressed with high yields (9-10 mg/L culture) in insect cells and eluted in two clean
472 peaks in SEC corresponding to a monomer and dimer, respectively. In the case of misfolding,
473 we would have expected aggregation and/or degradation during purification, and we would
474 not expect to see degradation of the zymogen in SDS-PAGE analysis only after addition of
475 Zn^{2+} which activates the metalloproteinase (Fig. 3e). Notably, the disintegrin domain of this
476 PII has 100% sequence identity to ocellatusin, a short, monomeric disintegrin of *Echis*
477 *ocellatus* venom (*52*). Previous studies have identified a discrepancy between the amounts

478 of ocellatusin and its PII-derived metalloproteinase in the venom, whereby ocellatusin
479 represents 3.9%, and the SVMP less than 0.1% of venom proteins (*3*). In summary, the
480 disintegrin is likely liberated from this PII SVMP and is the more pathogenic component of
481 the SVMP, causing inhibition of platelet aggregation (Fig. 5a). In contrast, the PII-derived
482 metalloproteinase domain is unstable and therefore requires high toxin concentrations to
483 elicit proteolytic activity in our activity assays (Fig. 4b,e).

484 The recombinant PIII zymogen was fully auto-activated in our experiments by the addition of
485 Zn^{2+} ions (Fig. 3f). Interestingly, this PIII SVMP was able to degrade its prodomain despite
486 the latter initially remaining bound to the mature protein according to SEC (Fig. 3c). This
487 agrees with the finding that prodomains, which are highly conserved in SVMPs, are rarely
488 identified in the venom proteome (*53*), suggesting that all prodomains might eventually be
489 fully degraded by venom proteases including PIII SVMPs.

490 Activated recombinant SVMPs were active against bovine casein, a general protease
491 substrate (Fig. 4a-c). PI and PIII exhibited strong activity, degrading all bands, while PII was
492 significantly less active, requiring much higher enzyme concentrations. This agrees with our
493 previous observation that bands corresponding to the MP-disintegrin protein or the MP
494 domain alone after activation with Zn^{2+} (Fig. 3e) are absent in SDS-PAGE, indicating that the
495 MP domain is likely unstable.

496 Fibrinogen degradation assays are particularly relevant for SVMPs and indicate their
497 potential haemotoxic activity (Fig. 4d-f). The 340 kDa fibrinogen glycoprotein is made up of
498 three pairs of polypeptide chains, which lead to three groups of distinct bands when
499 analysed by reducing SDS-PAGE: the Aα (70-75 kDa), Bβ (65 kDa) and γ (50 kDa) chains.
500 In contrast to the endogenous serine protease thrombin, which cleaves fibrinopeptides A and
501 B off the Aα and Bβ chains, causing self-polymerization into fibrin fibres and formation of
502 blood clots (*54*), the PI, PII, and PIII SVMPs studied here caused a fuller degradation of
503 fibrinogen (Fig. 4d-f). All SVMPs were active against both the Aα and Bβ chains of fibrinogen;
504 the PI and PIII showed a preference for the Aα chain and the PII preferentially degraded the
505 Bβ chain of fibrinogen. We conclude that the three SVMPs interfere with clot formation and
506 would thus contribute to an anticoagulant outcome upon envenoming. In agreement, the PIII
507 SVMP cannot cause clot formation in the thrombin clot time assay (Fig. 5d), suggesting it is
508 not an Ecarin-like prothrombin activator, which is typically responsible for procoagulant
509 activity seen in such assays with *Echis* venoms (Fig. 5c,e).

510 The recombinant PIII SVMP was highly active against a fluorogenic peptide substrate,
511 ES010, showing high affinity and specificity for cleavage of the Gly-Leu bond within the
512 peptide (Fig. 4g). In this context, we would like to point out that enzyme concentrations and
513 kinetics are based on zymogen concentrations, assuming 100% SVMP activation by Zn^{2+}

514 (Fig. 4a-g). If zymogen activations were incomplete or non-linear, our k_{cat}/K_M calculations
515 could either underestimate or overestimate the PIII SVMP's catalytic efficiency (Fig. 4g).

516 The SVMP PIII was also active against insulin B (Fig. 4h), as was SVMP PI (Fig. 4i) which
517 produced identical degradation products to native PI, confirming identical cleavage sites and
518 successful recombinant production of toxin with native-like characteristics, validating our
519 approach.

520 In addition to the proteolytic activity of the MP domain, PII and PIII SVMPs also include a
521 disintegrin or disintegrin-like domain containing a potential integrin binding motif. In platelet
522 aggregation assays, our RGD-containing PII SVMP inhibited 2-MeS-ADP-induced platelet-
523 aggregation with and without the prodomain present (Fig. 5a). The RSECD-containing PIII,
524 in contrast, did not inhibit 2-MeS-ADP-induced platelet aggregation, but this does not
525 exclude other disintegrin-like activity of this domain.

526 Zymogen expression was previously reported for ADAMs (A Disintegrin and
527 Metalloproteinases) and MMPs (Matrix Metalloproteinases), which are structurally and
528 functionally related to SVMPs. ADAMs and MMPs are involved in cell-cell interactions,
529 ectodomain shedding and degradation of extracellular matrix components respectively (*55*).
530 ADAMs and MMPs have become prominent targets in drug discovery (*56, 57*). For MMPs,
531 zymogen expression in mammalian and insect cells has been reported and enzyme
532 activation was achieved via 4-aminophenylmercuric acetate or trypsin to remove the
533 prodomain (*58, 59*). Moreover, ADAMs have been expressed with their prodomain to aid
534 proper folding and latency (*60, 61*). The ADAMs prodomain has been removed post-
535 translationally, e.g. by co-expression of furin (*62*). Interestingly, in agreement with our PI and
536 PIII SVMP observations, ADAM33 zymogen was processed and secreted in *Drosophila* S2
537 cells, with the prodomain remaining associated with the catalytic domain after purification.
538 The processing was enhanced by addition of cadmium chloride and zinc chloride (*63*). Auto-
539 activation of zymogens by Zn^{2+} incubation alone, however, has not been reported to the best
540 of our knowledge.

541 While ADAMs and MMPs are well characterized in the literature, comparable insights into
542 SVMPs were largely absent to date, due to lack of means for recombinant SVMP protein
543 production. Our generic protocol for recombinant SVMP zymogen production of all three
544 classes overcomes their high cytotoxicity and allows, for the first time, to study auto-
545 activation revealing important differences between the SVMP classes. Furthermore, our
546 protocol will unlock the production of many additional hitherto inaccessible SVMPs, allowing
547 in-depth characterization of their post-translational processing, enzymatic activity, substrate
548 specificity, cyto- and haemotoxicity, and enable the evaluation of potential biomedical
549 applications to develop new diagnostics and treatments for blood clotting disorders. Our

550 study paves the way to engineer existing and new SVMPs for improved and novel
551 applications in haematology, thrombosis, and inflammation research and other important
552 areas in which SVMPs can play a crucial role. Importantly, the recombinantly produced,
553 tagged SVMPs can serve as antigens for the future selection and evolution of neutralizing
554 antibodies as a basis for next-generation snakebite treatment to combat snakebite
555 envenomation.

556 **MATERIALS AND METHODS**

557 **SVMP expression construct design**

558 PI, PII and PIII SVMP constructs were designed by fusing an Avi- and His-tag
559 (GGSGLNDIFEAQKIEWHEHHHHHHHH*) to the C terminus of the native SVMP sequences
560 listed on UniProt (RRID: SCR_004426) (PI – Uniprot ID: Q2UXQ3, PII – Uniprot ID:
561 A0A3G1E3U2, PIII – Uniprot ID: E9JG34). The sequences were codon-optimized for
562 *Spodoptera frugiperda*, gene synthesized (Genscript) and inserted into the plasmid
563 pACEBac1 (Geneva Biotech), which acted as the donor in the MultiBac system (*64*).
564 Structure predictions of SVMP zymogens were performed using AlphaFold 3 (*30*) in the
565 presence of a single Zn^{2+}. Per residue predicted Local Distance Difference Test (pLDDT)
566 plots, indicating local confidence, were generated from B-factor values stored in the .cif files.
567 The highest-ranked model among the five predictions was selected for visualization and
568 figure generation using UCSF ChimeraX (RRID:SCR_015872,
569 https://www.cgl.ucsf.edu/chimerax/).

570 Mature SVMP constructs did not include the prodomain, but did contain an N-terminally
571 fused melittin signal sequence (MKFLVNVALVFMVVYISYIYA). Propeptide-SVMP fusions
572 contained an additional N-terminally fused propeptide triplicate and TEV site
573 (GGSPKMCGVTPKMCGVTPKMCGVTENLYFQSN) following the melittin signal sequence.
574 SVMP active site mutants were based on the mature SVMP constructs, but with the active
575 site glutamic acid mutated to aspartic acid and glycine mutated to cysteine (*65*). Zymogen
576 constructs comprised the native signal sequence preceding the native prodomain (which is
577 specific to the SVMP) and the SVMP sequence with a C-terminal Avi-His-tag fusion. PI was
578 found to undergo C-terminal processing, the site of which was predicted by modelling using
579 AlphaFold 3 (*30*). PI∆C construct contained the Avi-His-tag fusion following this site.

580 **Recombinant SVMP expression**

581 Each SVMP-containing pACEBac1 plasmid was expressed using the MultiBac
582 baculovirus/insect cell expression system following established protocols (*66*). SVMPs were
583 expressed in Hi5 insect cells at 19°C, in ESF 921 Insect Cell Culture Media (Expression
584 Systems). The cells were monitored throughout expression by measuring YFP fluorescence
585 (encoded in baculoviral genome) and cell viability (by determining percentage of alive cells
586 using Trypan Blue). A control expression of an unrelated, non-toxic protein (E3 ligase) was
587 used as a control for YFP and cell viability measurements. Expression in the presence of
588 Marimastat was tested using a final concentration of 0 μM, 3 μM and 6 μM Marimastat in the
589 cell culture media, which was added alongside the virus (at the start of expression). Cultures
590 were harvested 5 days after infection by centrifugation (1000 xg, 10 minutes), or when the

591 cell viability dropped below 80% if this occurred sooner. The secreted SVMP proteins were
592 purified immediately after harvesting from the supernatant.

593 **Western blotting**

594 Proteins resolved by SDS–PAGE were transferred to PVDF membranes (Trans-Blot Turbo
595 mini 0.2 µm PVDF Transfer Pack, Bio-Rad) using a Trans-Blot Turbo system for 7 min at
596 2.5 A and 25 V. Membranes were blocked in 2.5% (w/v) skimmed milk in PBST either
597 overnight at 4 °C or for 1 hour at room temperature, then washed three times for 5 min in
598 PBST. For detection of His-tagged proteins, membranes were incubated for 1 hour at room
599 temperature with HRP-conjugated anti-Penta-His antibody (diluted 1:2000 in PBS)
600 (QIAGEN), followed by PBST washes. For PDI detection, membranes were incubated
601 overnight at 4°C with rabbit anti-PDI antibody (Cell Signalling Technologies) diluted in PBS,
602 washed in PBST, and then incubated for 2 hours at room temperature with IRDye 680RD
603 Goat Anti-Rabbit IgG (diluted 1:10,000 in PBS) (LICORbio™), followed by further PBST
604 washes. Membranes were rinsed in PBS prior to imaging. His-tagged proteins were
605 visualized using SuperSignal™ West Pico PLUS Chemiluminescent Substrate (Thermo
606 Scientific) and the Synergene G: Box gel doc system, while PDI blots were imaged using a
607 fluorescence-based detection system in the Odyssey Fc Imager (LICORbio). Transfer
608 efficiency was assessed by Ponceau S staining following imaging.

609 **Co-expression of SVMPs with protein disulfide isomerase**

610 The PII and PIII SVMPs were additionally co-expressed with human or snake protein
611 disulfide isomerase (PDI) which was incorporated into the plasmid using Cre-lox (*67*). The
612 multigene expression construct was made using PDI-containing pIDC plasmids (Geneva
613 Biotech). pIDC_hPDI and pIDC_sPDI (PDI-insert synthetised by Genscript) as the donor
614 plasmids were fused with SVMP-containing pACEBac1 plasmids as the acceptor plasmid
615 (*67*). SVMP expression was carried out as above.

616 **Recombinant SVMP purification**

617 Clarified media (containing SVMP) was continuously passed through HiTrap IMAC FF 5 ml
618 column (Cytiva) at 2 ml/min, for 18 hours at 4ºC using a peristaltic pump. Subsequently, the
619 column was washed with 10 CV High Salt Buffer (50 mM Tris-Cl, 1 M NaCl, pH 8.0) and
620 10 CV SVMP Buffer (50 mM Tris-Cl, 300 mM NaCl, pH 8.0). After the washing steps, the
621 IMAC column was attached to an AKTA Pure system. The SVMP was eluted from the IMAC
622 column using a gradient of imidazole from 0 mM to 500 mM imidazole in SVMP buffer.
623 Fractions containing SVMP were pooled and dialyzed into SVMP Low Salt Buffer (50 mM
624 Tris-Cl, 50 mM NaCl, pH 8.0). SVMP was further purified by ion exchange chromatography
625 by passing the dialyzed protein through a 5 ml HiTrap Q XL column. Subsequently, the

626 SVMP was eluted from the column by a gradient of 50 mM to 1 M NaCl in SVMP buffer.
627 Fractions containing SVMP were pooled and concentrated to 500 µl (maximum 10 mg/ml).
628 Finally, SVMP was purified by size exclusion chromatography (SEC) using an Superdex 200
629 increase 10/300 GL column (Cytiva) in SVMP buffer with a flow rate of 0.375 ml/min. Cytiva
630 Gel Filtration Calibration Kits were used to calibrate the column, with elution peaks plotted to
631 generate a standard curve with which to calculate the molecular weights (MWs) of SVMP
632 proteins. Eluted SVMP was concentrated to 0.5 - 2 mg/ml using an Amicon concentrator with
633 appropriate MW cut off. Glycerol was added to 5% before the protein was flash frozen in
634 liquid nitrogen and stored at -80ºC.

635 **SVMP deglycosylation assay, PNGase F treatment**

636 Glycosylation of SVMP zymogens was determined by incubation with peptide-*N*-glycosidase
637 F (PNGase F, Promega) to remove N-linked oligosaccharide groups, followed by SDS-PAGE.
638 Briefly, the reaction was carried out with 1-2 µg SVMP diluted in 12 µl water, followed by
639 addition of 1 µl 5% SDS and 1 µl 1 M DTT. Next, the sample was heated at 95ºC for 5
640 minutes to denature the SVMP zymogens. Once cooled at room temperature, 2 µl SVMP
641 Buffer, 2 µl 10% NP-40 and 2 µl PNGase F were added. The reaction mix was incubated at
642 37ºC for 3 hours. Subsequently, SDS-PAGE sample buffer (reducing) was added, and the
643 samples were analysed by SDS-PAGE. SVMP zymogen deglycosylation was identified by a
644 shift towards lower MW of the SVMP band compared to the band where PNGase F was
645 omitted.

646 **Purification of PIII SVMP fraction from *Echis ocellatus* venom**

647 As a procoagulant control for blood clot time assays, an *Echis ocellatus* SVMP PIII fraction
648 was prepared using SEC. Whole venom (25 mg sourced from the herpetarium facility at the
649 Liverpool School of Tropical Medicine) was dissolved in 1.5 ml of PBS (25 mM sodium
650 phosphate, 150 mM NaCl, pH 7.2), centrifuged and the supernatant loaded onto a 120 ml
651 column of Superdex75 (Cytiva). Proteins were separated in PBS using a flow-rate of 1.0
652 ml/min and the separation was monitored at 280 nm. Two ml fractions were collected and
653 SDS-PAGE was used to determine the fractions containing SVMP PIIIs. These were pooled
654 and shown to be free of serine protease activity using the casein assay (see above) with
655 appropriate inhibitors.

656 **SVMP enzyme activation**

657 To determine optimal activation conditions, SVMP was titrated with 0 – 750 µM $ZnCl_2$, then
658 incubated at 26ºC or 37ºC for 18 hours. Activation was monitored using SDS-PAGE and
659 disappearance of the SVMP zymogen band in Coomassie-stained gels.

660 **Casein and fibrinogen degradation assays**

661 Activated SVMP was titrated into a freshly prepared 20 µl reaction mix containing casein or
662 fibrinogen at a final concentration of 0.525 mg/ml in SVMP Buffer. Final SVMP
663 concentrations ranged from 0 to 2.34 µM (based on SVMP zymogen concentration at the
664 start of the experiment). The negative control contained 5 mM EDTA as an SVMP inhibitor
665 and maximum concentrations of SVMP (PI - 2.34 µM, PII -1.07 and 1.34 µM, PIII - 685 nM).
666 Incubation was carried out at 37ºC for 18 hours. SDS-PAGE sample buffer was added, and
667 the samples were heated to 95ºC to stop the reaction, and the degradation pattern was
668 analysed by reducing SDS-PAGE.

669 **Fluorogenic peptide substrate cleavage assay**

670 The quenched fluorogenic peptide Mca-KPLGL-Dpa-AR-NH_2 (ES010, R&D systems Inc.)
671 was used to kinetically measure SVMP activity, whereby the activated SVMP cleaves the
672 Gly-Leu bond. Cleavage leads to the release of the Dpa-containing quencher from the
673 fluorescent Mca-containing fragment. ES010 substrate was diluted in reaction buffer (50 mM
674 Tris-Cl, 300 mM NaCl, pH 7.5) and used in the assay at final concentrations of 0 µM to
675 180 µM, in 100 µl in a 96 well plate. Enzymes were activated with Zn^{2+} (see above) and
676 added to a final concentration of 40 or 20 nM based on the SVMP zymogen concentration at
677 the start of the experiment. Fluorescence was followed for 30 minutes or 1 hour at 25ºC
678 using a BioTech Synergy Neo2 instrument, an excitation wavelength of 320 nm and emission
679 wavelength of 405 nm. Measurements were taken in triplicate. Kinetic data was plotted using
680 Origin (RRID:SCR_014212, https://www.originlab.com/index.aspx?go=PRODUCTS/Origin),
681 and a non-linear curve was fitted using the Michaelis-Menten function. Origin provided the
682 best-fit values for V_{max} and K_M, and k_{cat} could be calculated by V_{max}/enzyme concentration.
683 The fluorescence intensity versus time curve and the reaction rate were plotted and
684 calculated using GraphPad Prism 10.

685 **Insulin B degradation assay**

686 Insulin B degradation was determined following the established protocol (*15*), using a final
687 concentration of 0.02 mg/ml insulin B and 0.01 mg/ml activated SVMP, in 50 mM Tris-Cl, 150
688 mM NaCl, 1 mM $CaCl_2$, pH 7.5 (TBS) buffer. Incubation was carried out at 37ºC for 120
689 minutes, then trifluoracetic acid was added to 1% to stop the reaction. The whole sample (=
690 1 µg insulin B) was analysed by RP-HPLC using a C18 reverse phase column.

691 **Plate-based aggregometry**

692 Research involving derivatives of human blood samples was approved by the United Bristol
693 Healthcare NHS Trust Research Ethics Committee (project E5736), and all participants
694 provided written informed consent in accordance with the Declaration of Helsinki. Blood
695 samples were collected from healthy adult volunteers into 3.2% sodium citrate Vacutainer

696 tubes, and platelet-rich plasma (PRP) was prepared by centrifugation of citrated whole blood
697 at 180 × g for 17 minutes at room temperature. 2-MeS-ADP was prepared in HEPES-
698 Tyrode's buffer (10 mM HEPES pH 7.3, 145 mM NaCl, 1 mM $MgSO_4$, 3 mM KCl), and
699 experiments were performed using an end-point assay in 96-well half-area plates. 5 µL of
700 each SVMP (PI, PII, PIII and PII zymogen) were incubated with 45 µL PRP for 5 min at
701 37 °C prior to platelet aggregation induction by 2-MeS-ADP (2.5 µM). The plate was shaken
702 at 1200 rpm, 37 °C for 5 min, and the absorbance was then read at 595 nm using a Labtech
703 LT4500 plate reader. To determine % aggregation, the sample absorbance was normalized
704 accounting for unstimulated PRP as 0% aggregation, and the control (buffer without SVMP)
705 as 100% of aggregation. All means were calculated based on three assays performed in
706 duplicate. A two-way ANOVA was conducted, followed by simple effects analysis (Dunnett
707 post-test) to compare column means within each row, using GraphPad Prism 10.

708 **Bovine plasma clotting assay**

709 The assay was carried out following the protocol described by Still and colleagues (*68*).
710 Briefly, 20 µl activated SVMP or EchOce NGA (Nigerian *Echis ocellatus* venom) at 20 µg/ml
711 was added to 40 µl of 20 mM $CaCl_2$, and then 40 µl of citrated bovine plasma (Biowest
712 S0260-500) was added immediately before measuring absorbance at 595 nm on a
713 CLARIOstar Plus microplate reader. The clot formation was monitored for 30 minutes, at
714 room temperature. To obtain the normal clotting curve, 20 µl of PBS was added. For the no
715 clotting control, $CaCl_2$ was replaced with 20 µl of PBS. Absorbance versus time curves were
716 plotted using GraphPad Prism 10.

717 **Thrombin / SVMP clot time assay**

718 Experiments were carried out following manufacturer's kit instructions (HemosIL, Thrombin
719 Time 0009758515), using an ACL TOP coagulation analyser using 3.0 U/ml thrombin, 500 ng
720 PIII SVMP pool purified from *Echis ocellatus* venom and 500 ng activated recombinant PIII
721 SVMP. The assay measures the rate of increase in turbidity as the fibrin clot forms. The peak
722 in the rate of change (2nd derivative) is considered to be the point of clot formation.

723 **MTT cell viability assay**

724 MTT assay was based on the methods of Hall *et al.* (*47*). Immortalized human epidermal
725 keratinocytes, HaCaT (Caltag Medsystems, cells derived from a 62-year-old Caucasian male
726 donor's skin epidermis, RRID: CVCL_0038) were seeded (5,000 cells/well, clear-sided 96-
727 well plates) in standard medium (DMEM high glucose with GlutaMAX™ supplemented with 2
728 mM sodium pyruvate, 100 IU/ml penicillin, 250 µg/ml streptomycin, 10% Fetal Bovine Serum,
729 1% GlutaMAX™ (Thermo Fisher Scientific, #35050061)), then left to adhere overnight at
730 37°C, 5% CO_2. The cell line was freshly procured and checked for contamination before the

731 start of the experiment. The next day, the SVMPs treatments (25, 50 and 100 µg/ml) were
732 prepared in standard medium, and cells were treated with each prepared solution
733 (100 µl/well, duplicate wells) for 24 hours. For this assay, the MTT Cell Viability Assay Kit
734 (Biotium) was used: 10 µl of MTT solution was added to the 100 µl of medium in each well
735 and mixed by tapping gently on the side of the tray. The cells were incubated at 37 °C for 4
736 hours. 200 µl DMSO was added directly into the medium in each well and pipetted up and
737 down several times to dissolve the formazan salt. The absorbance was measured on BioTek
738 Synergy Neo2 spectrophotometer at 570 nm. The background absorbance was also
739 measured at 630 nm (subtracted background absorbance from signal absorbance to obtain
740 normalized absorbance values). The % of cell viability for each treatment well was calculated
741 as follows with buffer-treated cells as a control (100% viability):

742 $$\frac{Normalised\ abs\ treatment\ well\ - Average\ normalised\ abs\ blank\ wells}{Average\ normalised\ abs\ cell\ control\ wells - Average\ normalised\ abs\ blank\ wells}$$

743

744 **Materials availability**

745 Materials from this study are available from the corresponding authors upon reasonable
746 request.

747 **Acknowledgements**

748 The authors thank all members of the Berger, Schaffitzel and Casewell teams for
749 discussions and support. We gratefully acknowledge Loïc Quinton and Thomas Crasset
750 (University of Liège, Belgium) for their expert advice and insightful discussions on mass
751 spectrometry analyses of SVMPs.

752

753

754 **ADDITIONAL INFORMATION**

755 **Competing interests:** The authors declare that they have no competing interests.

756 **Funding**

Funder	Grant reference number	Author(s)
European Commission Horizon2020 FET OPEN	899670	C.S., I.B., R.V, N.R.C.
Wellcome Trust	221708/Z/20/Z	C.S, I.B. N.R.C.
UKRI Engineering Biology Mission Award	BB/Y007581/1	C.S, N.R.C.
EC Marie Sklodowska-Curie Fellowship	101149867; EP/Z002613/1	K.H.
Biotechnology and Biological Sciences Research Council, Studentships		I.A.C., S.L.
The funders had no role in study design, data collection, and interpretation, or the decision to submit the work for publication.		

757 **Author contributions**

758 Sophie Hall, methodology, data curation, formal analysis, investigation, writing – original
759 draft;

760 Iara Aimê Cardoso, methodology, data curation, formal analysis; Mark C. Wilkinson,
761 methodology, data curation, investigation formal analysis, writing - original draft; Maria
762 Molina Carretero, Srikanth Lingappa, Bronwyn Rand, Dakang Shen, data curation,
763 investigation; Johara Boldrini-França, methodology, writing – review and editing; Richard
764 Stenner, methodology; Stefanie K. Menzies, methodology; Georgia Balchin, Konrad Kamil
765 Hus, investigation; Renaud Vincentelli, investigation; Andrew Mumford, Alastair Poole,

supervision, writing - original draft; Nicholas R. Casewell, Supervision, writing - original draft; Imre Berger, conceptualization, methodology, supervision, writing - original draft; Christiane Schaffitzel, conceptualization, supervision, writing - original draft.

Author ORCIDs

Sophie Hall https://orcid.org/0000-0002-3176-6004

Iara Aimê Cardoso https://orcid.org/0000-0002-0288-4706

Mark C. Wilkinson https://orcid.org/0000-0003-3109-6888

Srikanth Lingappa https://orcid.org/0000-0002-0129-5512.

Bronwyn Rand https://orcid.org/0009-0008-0997-6217

Dakang Shen https://orcid.org/0009-0008-5327-1185

Johara Boldrini-França https://orcid.org/0000-0002-9444-7481

Richard Stenner https://orcid.org/0000-0003-0734-8686

Stefanie K. Menzies https://orcid.org/0000-0002-9273-9296

Georgia Balchin https://orcid.org/0009-0009-6944-6004

Konrad Kamil Hus https://orcid.org/0000-0003-2723-3691

Renaud Vincentelli https://orcid.org/0000-0001-9667-0196

Andrew Mumford https://orcid.org/0000-0002-5523-511X

Alastair W. Poole https://orcid.org/0000-0002-0868-297X

Nicholas R. Casewell https://orcid.org/0000-0002-8035-4719

Imre Berger https://orcid.org/0000-0001-7518-9045

Christiane Schaffitzel https://orcid.org/0000-0002-1516-9760

ADDITIONAL INFORMATION

Supplementary files

The supplementary information contains supplementary text and 11 additional supplementary figures.

Data availability

All data generated or analysed during this study are included in the manuscript and supporting files.

REFERENCES

1. A. L. Oliveira et al., The chemistry of snake venom and its medicinal potential. *Nat. Rev. Chem.* **6**, 451-469 (2022). https://doi.org/10.1038/s41570-022-00393-7
2. M. A. Bittenbinder et al., Tissue damaging toxins in snake venoms: mechanisms of action, pathophysiology and treatment strategies. *Commun. Biol.* **7**, 358 (2024). https://doi.org/10.1038/s42003-024-06019-6
3. S. C. Wagstaff, L. Sanz, P. Juarez, R. A. Harrison, J. J. Calvete, Combined snake venomics and venom gland transcriptomic analysis of the ocellated carpet viper, *Echis ocellatus. J. Proteomics* **71**, 609-623 (2009). https://doi.org/10.1016/j.jprot.2008.10.003
4. N. R. Casewell et al., Medically important differences in snake venom composition are dictated by distinct postgenomic mechanisms. *Proc. Natl. Acad. Sci. U.S.A.* **111**, 9205-9210 (2014). https://doi.org/10.1073/pnas.1405484111
5. T. Tasoulis, G. K. Isbister, A current perspective on snake venom composition and constituent protein families. *Arch. Toxicol.* **97**, 133-153 (2023). https://doi.org/10.1007/s00204-022-03420-0
6. J. W. Fox, S. M. Serrano, Insights into and speculations about snake venom metalloproteinase (SVMP) synthesis, folding and disulfide bond formation and their contribution to venom complexity. *FEBS J.* **275**, 3016-3030 (2008). https://www.ncbi.nlm.nih.gov/pubmed/18479462
7. N. R. Casewell, S. C. Wagstaff, R. A. Harrison, C. Renjifo, W. Wuster, Domain loss facilitates accelerated evolution and neofunctionalization of duplicate snake venom metalloproteinase toxin genes. *Mol. Biol. Evol.* **28**, 2637-2649 (2011). https://www.ncbi.nlm.nih.gov/pubmed/21478373
8. A. F. Asega et al., Cleavage of proteoglycans, plasma proteins and the platelet-derived growth factor receptor in the hemorrhagic process induced by snake venom metalloproteinases. *Sci. Rep.* **10**, 12912 (2020). https://doi.org/10.1038/s41598-020-69396-y
9. R. M. Kini, C. Y. Koh, Metalloproteases Affecting Blood Coagulation, Fibrinolysis and Platelet Aggregation from Snake Venoms: Definition and Nomenclature of Interaction Sites. *Toxins (Basel)* **8** (2016). https://doi.org/10.3390/toxins8100284
10. J. M. Gutierrez, A. Rucavado, T. Escalante, C. Diaz, Hemorrhage induced by snake venom metalloproteinases: biochemical and biophysical mechanisms involved in microvessel damage. *Toxicon* **45**, 997-1011 (2005). https://doi.org/10.1016/j.toxicon.2005.02.029
11. J. M. Gutierrez, T. Escalante, A. Rucavado, C. Herrera, J. W. Fox, A Comprehensive View of the Structural and Functional Alterations of Extracellular Matrix by Snake Venom Metalloproteinases (SVMPs): Novel Perspectives on the Pathophysiology of Envenoming. *Toxins (Basel)* **8** (2016). https://doi.org/10.3390/toxins8100304

817 12. G. O. Almeida, I. S. de Oliveira, E. C. Arantes, S. V. Sampaio, Snake venom disintegrins
818 update: insights about new findings. *J. Venom. Anim. Toxins Incl. Trop. Dis.* **29**,
819 e20230039 (2023). https://doi.org/10.1590/1678-9199-JVATITD-2023-0039

820 13. G. W. Moore, Snake Venoms in Diagnostic Hemostasis and Thrombosis. *Semin.*
821 *Thromb. Hemost.* **48**, 145-160 (2022). https://doi.org/10.1055/s-0041-1732465

822 14. J. Slagboom, J. Kool, R. A. Harrison, N. R. Casewell, Haemotoxic snake venoms: their
823 functional activity, impact on snakebite victims and pharmaceutical promise. *Br. J.*
824 *Haematol.* **177**, 947-959 (2017). https://doi.org/10.1111/bjh.14591

825 15. M. C. Wilkinson et al., Complex compositional and functional diversity of venom
826 metalloproteinases in African puff adders. bioRxiv, 2024.2005.2031.596867 (2025).
827 https://doi.org/10.1101/2024.05.31.596867

828 16. K. T. Yee, M. Pitts, P. Tongyoo, P. Rojnuckarin, M. C. Wilkinson, Snake Venom
829 Metalloproteinases and Their Peptide Inhibitors from Myanmar Russell's Viper Venom.
830 *Toxins (Basel)* **9** (2016). https://doi.org/10.3390/toxins9010015

831 17. O. T. Olaoba, P. Karina Dos Santos, H. S. Selistre-de-Araujo, D. H. Ferreira de Souza,
832 Snake Venom Metalloproteinases (SVMPs): A structure-function update. *Toxicon X* **7**,
833 100052 (2020). https://doi.org/10.1016/j.toxcx.2020.100052

834 18. A. Pinyachat, P. Rojnuckarin, C. Muanpasitporn, P. Singhamatr, S. Nuchprayoon,
835 Albocollagenase, a novel recombinant P-III snake venom metalloproteinase from green
836 pit viper (*Cryptelytrops albolabris*), digests collagen and inhibits platelet aggregation.
837 *Toxicon* **57**, 772-780 (2011). https://doi.org/10.1016/j.toxicon.2011.02.011

838 19. M. T. Assakura, C. A. Silva, R. Mentele, A. C. Camargo, S. M. Serrano, Molecular
839 cloning and expression of structural domains of bothropasin, a P-III metalloproteinase
840 from the venom of *Bothrops jararaca. Toxicon* **41**, 217-227 (2003).
841 https://doi.org/10.1016/s0041-0101(02)00279-9

842 20. A. Jonebring et al., Expression and characterization of recombinant Ecarin. *Protein J.* **31**,
843 353-358 (2012). https://doi.org/10.1007/s10930-012-9409-6

844 21. K. Shimokawa, L. G. Jia, X. M. Wang, J. W. Fox, Expression, activation, and processing
845 of the recombinant snake venom metalloproteinase, pro-atrolysin E. *Arch. Biochem.*
846 *Biophys.* **335**, 283-294 (1996). https://doi.org/10.1006/abbi.1996.0509

847 22. E. Camacho, T. Escalante, K. Remans, J. M. Gutierrez, A. Rucavado, Site mutation of
848 residues in a loop surrounding the active site of a PI snake venom metalloproteinase
849 abrogates its hemorrhagic activity. *Biochem. Biophys. Res. Commun.* **512**, 859-863
850 (2019). https://doi.org/10.1016/j.bbrc.2019.03.152

851 23. C. Bieniossek, T. Imasaki, Y. Takagi, I. Berger, MultiBac: expanding the research toolbox
852 for multiprotein complexes. *Trends Biochem. Sci.* **37**, 49-57 (2012).
853 https://doi.org/10.1016/j.tibs.2011.10.005

854 24. O. B. Villaflores et al., Easy expression of the C-terminal heavy chain domain of
855 botulinum neurotoxin serotype A as a vaccine candidate using a bi-cistronic baculovirus

856 system. *J. Virol. Methods* **189**, 58-64 (2013).
857 https://doi.org/10.1016/j.jviromet.2012.11.035

858 25. J. K. A. Macêdo, Fox, J.W., Biological Activities and Assays of the Snake Venom
859 Metalloproteinases (SVMPs). In *Venom Genomics and Proteomics. Toxinology.* (ed.
860 Gopalakrishnakone, P., Calvete, J.) (Springer, 2016). https://doi.org/10.1007/978-94-
861 007-6416-3_21

862 26. J. Alsolaiss, N. Alomran, L. Hawkins, N. R. Casewell, Commercial Antivenoms Exert
863 Broad Paraspecific Immunological Binding and *In Vitro* Inhibition of Medically Important
864 *Bothrops* Pit Viper Venoms. *Toxins (Basel)* **15** (2022).
865 https://doi.org/10.3390/toxins15010001

866 27. D. Redureau et al., Dual Proteomics Strategies to Dissect and Quantify the Components
867 of Nine Medically Important African Snake Venoms. *Toxins (Basel)* **17** (2025).
868 https://doi.org/10.3390/toxins17050243

869 28. D. C. Tessier, D. Y. Thomas, H. E. Khouri, F. Laliberte, T. Vernet, Enhanced secretion
870 from insect cells of a foreign protein fused to the honeybee melittin signal peptide. *Gene*
871 **98**, 177-183 (1991). https://doi.org/10.1016/0378-1119(91)90171-7

872 29. F. Grams, R. Huber, L. F. Kress, L. Moroder, W. Bode, Activation of snake venom
873 metalloproteinases by a cysteine switch-like mechanism. *FEBS Lett*. **335**, 76-80 (1993).
874 https://doi.org/10.1016/0014-5793(93)80443-x

875 30. J. Abramson et al., Accurate structure prediction of biomolecular interactions with
876 AlphaFold 3. *Nature* **630**, 493-500 (2024). https://doi.org/10.1038/s41586-024-07487-w

877 31. S. P. Mackessy, L.M. Baxter, Bioweapons synthesis and storage: The venom gland of
878 front-fanged snakes. *Zoologischer Anzeiger - A Journal of Comparative Zoology* **245**,
879 147-159 (2006). https://doi.org/10.1016/j.jcz.2006.01.003

880 32. E. F. Sanchez et al., The novel metalloproteinase atroxlysin-I from Peruvian *Bothrops*
881 *atrox* (Jergon) snake venom acts both on blood vessel ECM and platelets. *Arch.*
882 *Biochem. Biophys.* **496**, 9-20 (2010). https://doi.org/10.1016/j.abb.2010.01.010

883 33. C. A. Bello et al., Isolation and biochemical characterization of a fibrinolytic proteinase
884 from *Bothrops leucurus* (white-tailed jararaca) snake venom. *Biochimie* **88**, 189-200
885 (2006). https://doi.org/10.1016/j.biochi.2005.07.008

886 34. C. P. Bernardes et al., Isolation and structural characterization of a new fibrin(ogen)olytic
887 metalloproteinase from *Bothrops moojeni* snake venom. *Toxicon* **51**, 574-584 (2008).
888 https://doi.org/10.1016/j.toxicon.2007.11.017

889 35. R. Gupta, S. Brunak, Prediction of glycosylation across the human proteome and the
890 correlation to protein function. *Pac. Symp. Biocomput.* 310-322 (2002).
891 https://www.ncbi.nlm.nih.gov/pubmed/11928486

892 36. I. L. Junqueira-de-Azevedo et al., Venom-related transcripts from *Bothrops jararaca*
893 tissues provide novel molecular insights into the production and evolution of snake
894 venom. *Mol. Biol. Evol.* **32**, 754-766 (2015). https://doi.org/10.1093/molbev/msu337

895 37. H. Safavi-Hemami et al., Rapid expansion of the protein disulfide isomerase gene family
896 facilitates the folding of venom peptides. *Proc. Natl. Acad. Sci. U.S.A.* **113**, 3227-3232
897 (2016). https://doi.org/10.1073/pnas.1525790113

898 38. T. A. Hsu, S. Watson, J. J. Eiden, M. J. Betenbaugh, Rescue of immunoglobulins from
899 insolubility is facilitated by PDI in the baculovirus expression system. *Protein Expr. Purif.*
900 **7**, 281-288 (1996). https://doi.org/10.1006/prep.1996.0040

901 39. G. T. T. Nguyen et al., High-throughput proteomics and *in vitro* functional
902 characterization of the 26 medically most important elapids and vipers from sub-
903 Saharan Africa. *Gigascience* **11** (2022). https://doi.org/10.1093/gigascience/giac121

904 40. A. Azevedo, A. F. Prado, J. P. Issa, R. F. Gerlach, Matrix metalloproteinase 2 fused to
905 GFP, expressed in *E. coli*, successfully tracked MMP-2 distribution *in vivo*. *Int. J. Biol.*
906 *Macromol.* **89**, 737-745 (2016). https://doi.org/10.1016/j.ijbiomac.2016.05.013

907 41. P. Schlage, T. Kockmann, F. Sabino, J. N. Kizhakkedathu, U. Auf dem Keller, Matrix
908 Metalloproteinase 10 Degradomics in Keratinocytes and Epidermal Tissue Identifies
909 Bioactive Substrates With Pleiotropic Functions. *Mol. Cell. Proteomics* **14**, 3234-3246
910 (2015). https://doi.org/10.1074/mcp.M115.053520

911 42. W. J. Akers et al., Detection of MMP-2 and MMP-9 activity *in vivo* with a triple-helical
912 peptide optical probe. *Bioconjug. Chem.* **23**, 656-663 (2012).
913 https://doi.org/10.1021/bc300027y

914 43. J. M. Howes, M. C. Wilkinson, R. D. Theakston, G. D. Laing, The purification and partial
915 characterisation of two novel metalloproteinases from the venom of the West African
916 carpet viper, *Echis ocellatus*. *Toxicon* **42,** 21-27 (2003). https://doi.org/10.1016/S0041-
917 0101(03)00096-5

918 44. S. Takeda, H. Takeya, S. Iwanaga, Snake venom metalloproteinases: structure, function
919 and relevance to the mammalian ADAM/ADAMTS family proteins. *Biochim. Biophys.*
920 *Acta* **1824**, 164-176 (2012). https://doi.org/10.1016/j.bbapap.2011.04.009

921 45. T. Mosmann, Rapid colorimetric assay for cellular growth and survival: application to
922 proliferation and cytotoxicity assays. *J. Immunol. Methods* **65**, 55-63 (1983).
923 https://doi.org/10.1016/0022-1759(83)90303-4

924 46. R. D. Pierce et al., Characterization of crude *Echis carinatus* venom-induced cytotoxicity
925 in HEK 293T cells. *J. Venom Res.* **2**, 59-67 (2011).
926 https://www.ncbi.nlm.nih.gov/pubmed/22331993

927 47. S. R. Hall et al., Repurposed drugs and their combinations prevent morbidity-inducing
928 dermonecrosis caused by diverse cytotoxic snake venoms. *Nat. Commun.* **14**, 7812
929 (2023). https://doi.org/10.1038/s41467-023-43510-w

930 48. J. A. Portes-Junior et al., Unraveling the processing and activation of snake venom
931 metalloproteinases. *J. Proteome Res.* **13**, 3338-3348 (2014).
932 https://www.ncbi.nlm.nih.gov/pubmed/24914619w

933 49. S. M. Carneiro et al., Immunolocalization of venom metalloproteases in venom glands of
934 adult and of newborn snakes of *Bothrops jararaca. Tissue Cell* **34**, 381-389 (2002).
935 https://www.ncbi.nlm.nih.gov/pubmed/12441090

936 50. S. Watanabe et al., Sialylation of N-glycans on the recombinant proteins expressed by a
937 baculovirus-insect cell system under beta-N-acetylglucosaminidase inhibition. *J. Biol.*
938 *Chem.* **277**, 5090-5093 (2002). https://www.ncbi.nlm.nih.gov/pubmed/11741890

939 51. D. Andrade-Silva et al., Structures of N-Glycans of Bothrops Venoms Revealed as
940 Molecular Signatures that Contribute to Venom Phenotype in Viperid Snakes. *Mol. Cell*
941 *Proteomics* **17**, 1261-1284 (2018). https://www.ncbi.nlm.nih.gov/pubmed/29716988

942 52. J. B. Smith et al., Characterization of a monomeric disintegrin, ocellatusin, present in the
943 venom of the Nigerian carpet viper, *Echis ocellatus. FEBS Lett.* **512**, 111-115 (2002).
944 https://www.ncbi.nlm.nih.gov/pubmed/11852062

945 53. A. M. Moura-da-Silva et al., Processing of Snake Venom Metalloproteinases:
946 Generation of Toxin Diversity and Enzyme Inactivation. *Toxins (Basel)* **8** (2016).
947 https://doi.org/10.3390/toxins8060183

948 54. J. W. Weisel, R. I. Litvinov, Fibrin Formation, Structure and Properties. *Subcell. Biochem.*
949 **82**, 405-456 (2017). https://doi.org/10.1007/978-3-319-49674-0_13son

950 55. S. Takeda, ADAM and ADAMTS Family Proteins and Snake Venom Metalloproteinases:
951 A Structural Overview. *Toxins (Basel)* **8** (2016). https://doi.org/10.3390/toxins8050155

952 56. C. M. Overall, C. Lopez-Otin, Strategies for MMP inhibition in cancer: innovations for the
953 post-trial era. *Nat. Rev. Cancer* **2**, 657-672 (2002). https://doi.org/10.1038/nrc884

954 57. V. J. Craig, L. Zhang, J. S. Hagood, C. A. Owen, Matrix metalloproteinases as
955 therapeutic targets for idiopathic pulmonary fibrosis. *Am. J. Respir. Cell. Mol. Biol.* **53**,
956 585-600 (2015). https://doi.org/10.1165/rcmb.2015-0020TR

957 58. Y. Ogata, Y. Itoh, H. Nagase, Steps involved in activation of the pro-matrix
958 metalloproteinase 9 (progelatinase B)-tissue inhibitor of metalloproteinases-1 complex
959 by 4-aminophenylmercuric acetate and proteinases. *J. Biol. Chem.* **270**, 18506-18511
960 (1995). https://doi.org/10.1074/jbc.270.31.18506

961 59. R. Vallon, R. Müller, D. Moosmayer, E. Gerlach, P. Angel, The catalytic domain of
962 activated collagenase I (MMP-1) is absolutely required for interaction with its specific
963 inhibitor, tissue inhibitor of metalloproteinases-1 (TIMP-1). *Eur. J. Biochem.* **244**, 81-88
964 (1997). https://doi.org/10.1111/j.1432-1033.1997.00081.x

965 60. G. C. Jones, M. N. Vankemmelbeke, D. J. Buttle, Expression of recombinant ADAMTS
966 in insect cells. *Methods Mol. Biol.* **622**, 83-98 (2010). https://doi.org/10.1007/978-1-
967 60327-299-5_5

968 61. A. Chavaroche et al., Glycosylation of a disintegrin and metalloprotease 17 affects its
969 activity and inhibition. *Anal. Biochem.* **449**, 68-75 (2014).
970 https://doi.org/10.1016/j.ab.2013.12.018

971 62. E. Wong, T. Maretzky, Y. Peleg, C. P. Blobel, I. Sagi, The Functional Maturation of A
972 Disintegrin and Metalloproteinase (ADAM) 9, 10, and 17 Requires Processing at a
973 Newly Identified Proprotein Convertase (PC) Cleavage Site. *J. Biol. Chem.* **290**, 12135-
974 12146 (2015). https://doi.org/10.1074/jbc.M114.624072

975 63. W. W. Prosise et al., Protease domain of human ADAM33 produced by *Drosophila* S2
976 cells. *Protein Expr. Purif.* **38**, 292-301 (2004). https://doi.org/10.1016/j.pep.2004.09.004

977 64. D. Sari et al., The MultiBac Baculovirus/Insect Cell Expression Vector System for
978 Producing Complex Protein Biologics. *Adv. Exp. Med. Biol.* **896**, 199-215 (2016).
979 https://doi.org/10.1007/978-3-319-27216-0_13

980 65. E. Camacho et al., Novel Catalytically-Inactive PII Metalloproteinases from a Viperid
981 Snake Venom with Substitutions in the Canonical Zinc-Binding Motif. *Toxins (Basel)* **8**,
982 (2016). https://www.ncbi.nlm.nih.gov/pubmed/27754342

983 66. D. Sari-Ak et al., VLP-factory and ADDomer: Self-assembling Virus-Like Particle (VLP)
984 Technologies for Multiple Protein and Peptide Epitope Display. *Curr. Protoc.* **1**, e55
985 (2021). https://doi.org/10.1002/cpz1.55

986 67. M. Haffke, C. Viola, Y. Nie, I. Berger, Tandem recombineering by SLIC cloning and Cre-
987 LoxP fusion to generate multigene expression constructs for protein complex research.
988 *Methods Mol. Biol.* **1073**, 131-140 (2013). https://doi.org/10.1007/978-1-62703-625-2_11

989 68. K. B. M. Still et al., Multipurpose HTS Coagulation Analysis: Assay Development and
990 Assessment of Coagulopathic Snake Venoms. *Toxins (Basel)* **9**, (2017).
991 https://www.ncbi.nlm.nih.gov/pubmed/29186818
992

993 **FIGURES AND LEGENDS**

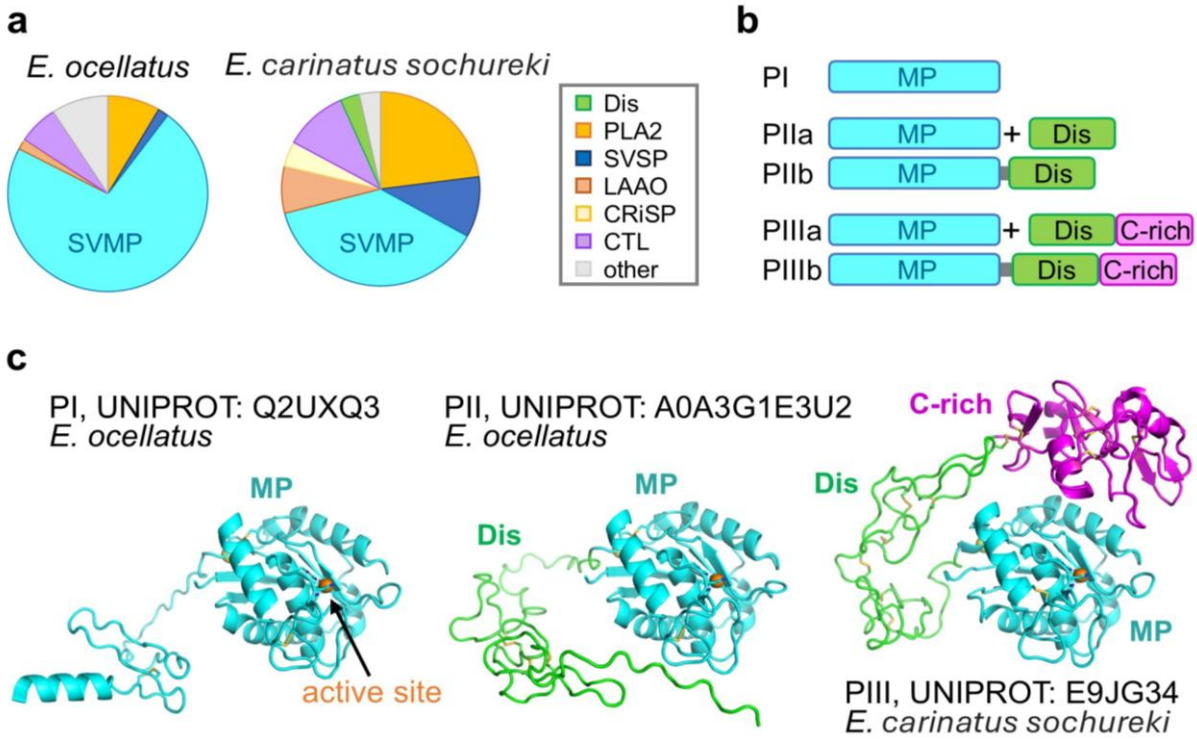

994

995 **Figure 1: SVMP classification and abundance in *Echis* venom.** (**a**) Pie charts displaying
996 *Echis ocellatus* and *Echis carinatus sochureki* venom composition, with SVMP coloured in
997 cyan (*1*). (**b**) Simplified schematic of mature PI, PII and PIII SVMP architecture, showing
998 metalloproteinase domain (MP, cyan), disintegrin domain (Dis, green) and cysteine-rich
999 domain (C-rich, magenta). (**c**) AlphaFold 3 predicted structural models of PI and PII SVMPs
1000 from *Echis ocellatus*, and PIII SVMP from *Echis carinatus sochureki*. Domain names and
1001 colour coding as in panel b. Zn^{2+} ions (orange) in the active site are shown as spheres.

1002

1003

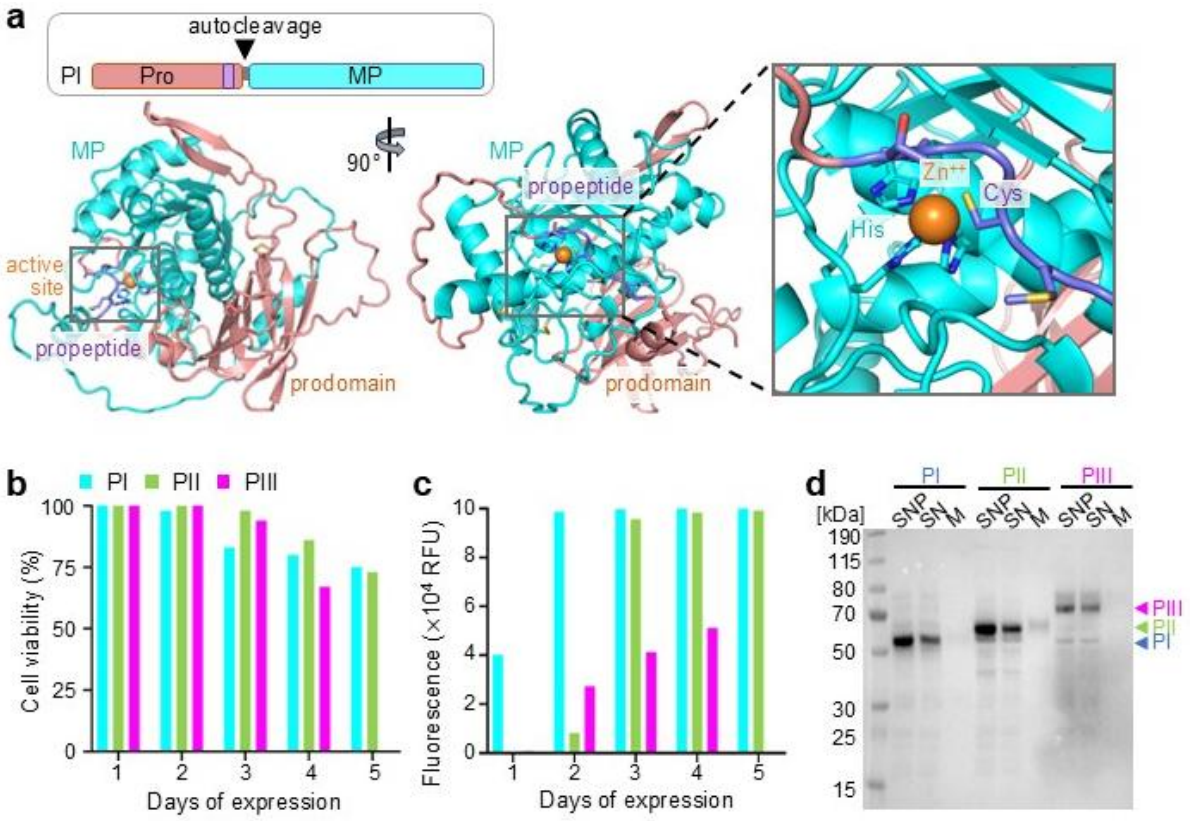

1004

1005 **Figure 2: PI, PII and PIII SVMP zymogen expression.** (**a**) Above: Schematic of PI SVMP
1006 zymogen with N-terminal prodomain (Pro, salmon), propeptide (purple). Below: left: two
1007 views of AlphaFold 3 prediction of PI zymogen model; right: zoom in on active site Zn^{2+} ion
1008 coordinated by histidines and propeptide cysteine. Expression of SVMP zymogens
1009 monitored by (**b**) cell viability, (**c**) YFP fluorescence (PIII harvested on day 4), (**d**) Western
1010 blot analysis using HRP-conjugated anti-Penta-His antibody. SNP: supernatant+pellet, SN:
1011 supernatant, M: media (10x concentrated). Grey bars: non-toxic protein expression control,
1012 cyan: PI SVMP, green: PII SVMP, magenta: PIII SVMP. SVMP zymogen expression was
1013 repeated five times.

1014

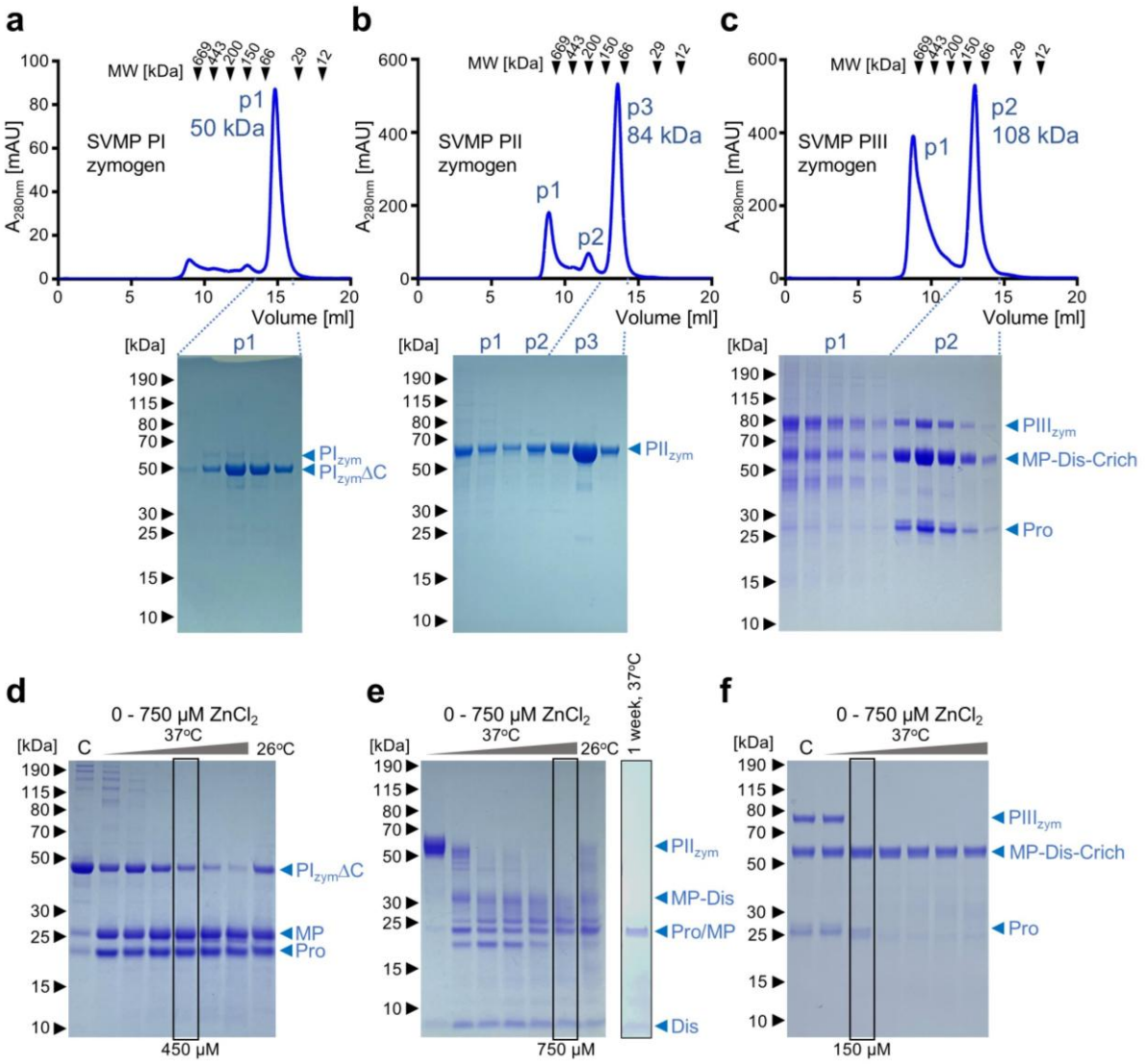

Figure 3: SEC purification of SVMP zymogens and auto-activation. Size exclusion chromatograms and SDS-PAGE of (**a**) PI zymogen ($PI_{zym}\Delta C$ lacks C-terminal tags), (**b**) PII zymogen, and (**c**) PIII zymogen after IMAC and IEX. $PIII_{zym}$ partial cleavage separates the prodomain (Pro) and the mature PIII. Elution volumes of MW calibration markers are indicated in the chromatograms as black arrows. (**d**) Activation of PI zymogen into metalloproteinase and prodomain. C (control): no 18-hour incubation. (**e**) Activation of PII zymogen into metalloproteinase-disintegrin and disintegrin domain (prodomain cannot be definitively identified). After 1 week only 8 kDa and 23 kDa bands remain. (**f**) Activation of PIII zymogen into prodomain and mature PIII. At higher Zn^{2+} concentrations, the prodomain is degraded. C (control): no 18-hour incubation. SVMP zymogen purifications and activations were repeated five times.

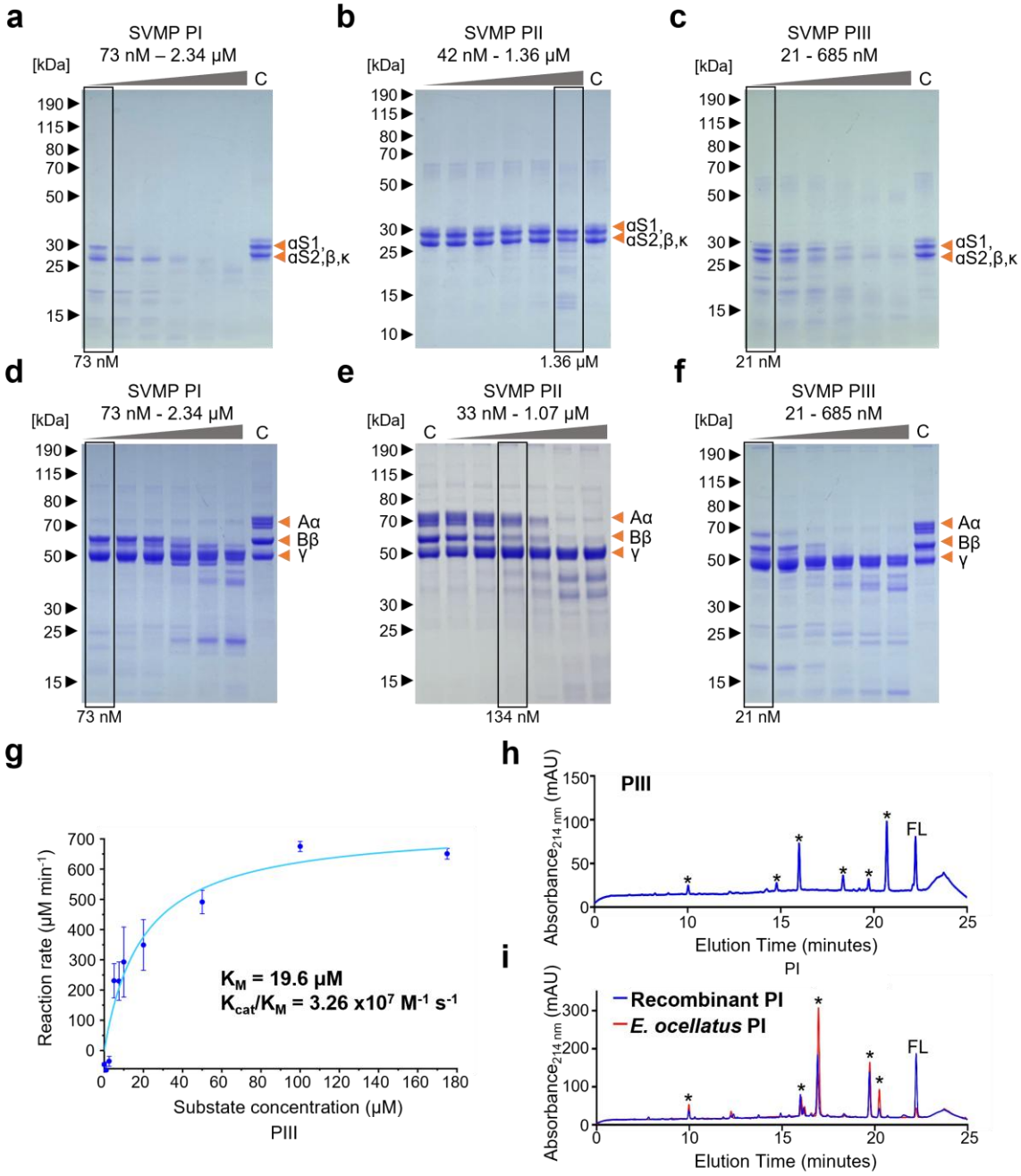

1027

1028 **Figure 4: *In vitro* SVMP activity and substrate specificity.** Casein degradation in the
1029 presence of increasing amounts of (**a**) PI, (**b**) PII and (**c**) PIII SVMPs. Orange arrowheads:
1030 domains αS1, αS2, β and κ. Fibrinogen degradation in the presence of increasing amounts
1031 of (**d**) PI, (**e**) PII and (**f**) PIII. Orange arrowheads: fibrinogen chains Aα, Bβ and γ. C (control):
1032 incubation in the presence of 5 mM EDTA. (**g**) PIII SVMP (20 nM) activity towards the
1033 fluorogenic peptide substrate ES010. (**h,i**) Degradation of insulin B by (**h**) PIII and (**i**)
1034 recombinant (blue) and *Echis ocellatus* PI (red). Full-length insulin (FL) and degradation
1035 products (*) are marked above the peaks. All degradation assays were repeated three times.
1036 The fluorogenic peptide assay shows the result of three independent repeats.

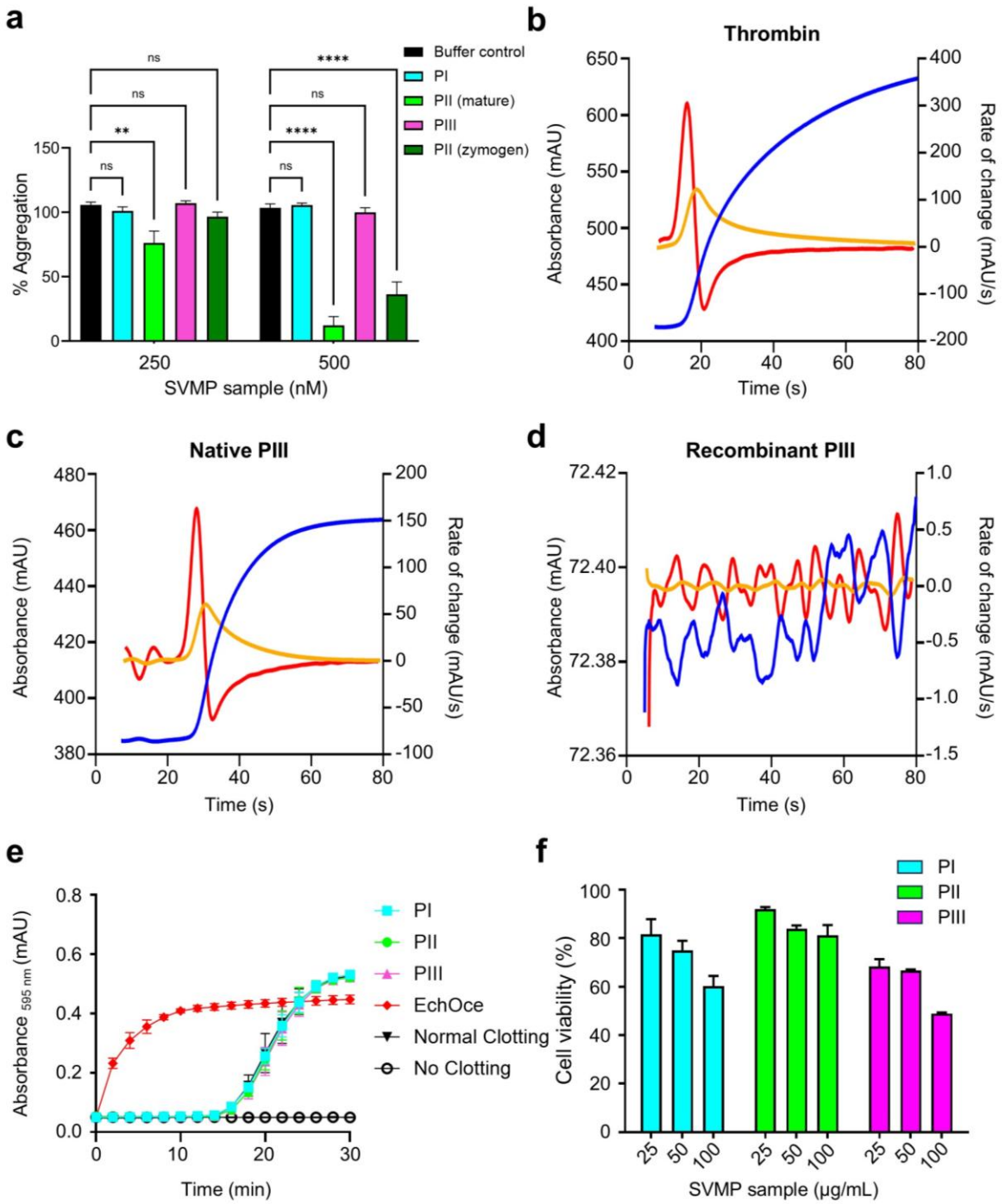

1037

1038 **Figure 5: SVMP blood coagulation, platelet aggregation and cytotoxicity.** (**a**) Inhibition
1039 of platelet aggregation by PI, PII (mature and zymogen) and PIII. Control: PRP with buffer.
1040 Data are presented as the mean of % aggregation ± SEM. A two-way ANOVA was conducted,
1041 followed by simple effects analysis (Dunnett post-test) to compare column means (SVMPs)
1042 within each row (concentrations). ****: $p \leq 0.0001$, **: $p \leq 0.01$. The assay was carried out in
1043 experimental duplicate and biological triplicate. (**b**)-(**d**) Thrombin clot time assays using the
1044 ACL TOP coagulation analyser. Citrated human blood was spiked with (**b**) thrombin, (**c**) a
1045 pool of native *Echis ocellatus* PIII SVMPs, and (**d**) the recombinant PIII SVMP. Change in
1046 absorbance (blue) is plotted on the left Y axis, rate of change (1st derivative: orange; 2nd

1047 derivative: red) is plotted on the right Y axis. Assays were repeated three times. (**e**)
1048 Coagulation profiles of the recombinant SVMPs and *Echis ocellatus* venom in bovine plasma
1049 over 30 minutes at an absorbance of 595 nm. Data points represent the mean of three
1050 individual values ± SD. The experiment was repeated two times. (**f**) MTT cytotoxicity assay
1051 showing viability compared to the buffer-only control of HaCaT cells after 24-hour incubation
1052 with activated PI, PII and PIII SVMPs. Bars show the results of two independent repeats.